Seasonal variability and estuary-shelf interactions in circulation dynamics of a river- dominated estuary

Arun Chawla [1*], David A. Jay [2], António M. Baptista [3], Michael Wilkin [3] and Charles Seaton [3]

[1] *Environmental & Biomolecular Systems*
Oregon Health & Science University
Beaverton OR 97006
(presently at NCEP, MD)

[2] *Department of Civil & Environmental Engineering*
Portland State University
Portland OR 97207
djay@cecs.pdx.edu

[3] *Science and Technology Center for Coastal Margin Observation and Prediction*
Oregon Health & Science University
Beaverton OR 97006

[*] *Corresponding author; Ph:301-763-8000 x 7209; Fax:301-763-8545; e-mail:arun.chawla@noaa.gov*

Abstract

The long-term response of circulation processes to external forcing has been quantified for the Columbia River estuary using in-situ data from an existing coastal observatory. Circulation patterns were determined from four Acoustic Doppler Profilers (ADP) and several conductivity-temperature sensors placed in the two main channels. Due to the very strong river discharge, baroclinic processes play a crucial role in the circulation dynamics, and the interaction of the tidal and subtidal baroclinic pressure gradients plays a major role in structuring the velocity field. The input of river flow and the resulting low-frequency flow dynamics in the two channels are quite distinct. Current and salinity data were analyzed on two time scales – sub tidal (or residual) and tidal (both diurnal and semidiurnal components). The residual currents in both channels usually showed a classical two-layer baroclinic circulation system with inflow at the bottom and outflow near the surface. However this two-layer system is transient and breaks down under strong discharge and tidal conditions, due to enhanced vertical mixing. Influence of shelf winds on estuarine processes was also observed via the interactions with upwelling and downwelling processes and coastal plume transport. The transient nature of residual inflow affects the long-term transport characteristics of the estuary. Effects of vertical mixing could also be seen at the tidal time-scale. Tidal velocities were separated into their diurnal and semidiurnal components using continuous wavelet transforms to account for the non-stationary nature of velocity amplitudes. The vertical structure of velocity amplitudes were considerably altered by baroclinic gradients. This was particularly true for the diurnal components, where tidal asymmetry led to stronger tidal velocities near the bottom.

1 Introduction

Circulation dynamics play a critical role in estuarine physical, chemical and biological transport processes, and a proper understanding of these dynamics provides the baseline for further scientific studies. Theoretical analyses typically assume that circulation processes can be separated into barotropic (Ianiello 1977, Li and O'Donnell 1997) and baroclinic (Hansen and Rattray, 1965) components, and that these can be quantified separately. Interactions between the tidal and residual flows are, in theoretical treatments, limited or sometimes absent. This approach has proved useful in partially mixed estuaries with weak tidal forcings, where circulation processes are predominantly stationary. However, several studies (Geyer 1988, Simpson *et al.* 1990, Jay and Smith 1990c, Jay and Musiak 1996, Monismith and Fong 1996) have shown that in river-dominated estuaries, internal tidal asymmetry (ebb-flood asymmetry in density gradients) plays a crucial role in the development of residual currents and important features such as the neap-spring fluctuation in residual flow profiles (Jay and Smith 1990a, 1990b) can only be explained by coupling the barotropic and baroclinic circulation dynamics. The influence of baroclinic processes is not limited to residual scales, with these processes being able to alter the vertical profile of tidal currents as well (Davies, 1993 and Jay and Musiak 1996).

The development of estuarine baroclinic circulation depends on the salinity distribution and the dynamics of salt transport, which in turn are strongly dependent on the circulation. Variable external forcings can then lead to a highly non-stationary environment in river-dominated estuaries where baroclinic circulation forms a significant proportion of the total estuarine circulation. In such systems, circulation dynamics are influenced by a combination of external forcing (winds, river discharge and tides) as well as internal mixing. The variability in transport processes thus depends to a large extent on the variability of the external forcings. The Columbia River estuary illustrates this point very well. Fig. 1 shows, for comparable tidal conditions, the salt wedge intrusion into the estuary during the spring freshets of 1997 (which had the strongest freshet since 1974) and 2001, a very low-flow year. During 1997, the flow was four times higher, and the salt wedge intruded less than half as far as in 2001. Horizontal and vertical density gradients were also much sharper during the high flow year. Such sharp density gradients play a

critical role in circulation processes.

The challenge is to determine how the fluctuations in the external forcing affect circulation in different parts of the estuary. Here, we address three questions:

- What are the seasonal and interannual variations in the tidal and subtidal circulation patterns?
- How do tidal processes affect residual flows and the salinity distribution?
- What are the exchange mechanisms between the shelf and the estuary?

With the above questions in mind, this study examines long term circulation and salinity records from the Columbia River Ecosystem CORIE (Baptista *et al*. 1999, Baptista 2006) and identifies the important physical processes involved.

2 Setting: the Columbia River and Estuary

The Columbia River system as considered here includes the estuary and tidal river (to the head of the tide at Bonneville dam, km-260) and extends offshore to the continental shelf where the influence of the fresh water plume from the Columbia River can be felt. The estuary itself is shallow and meso-tidal with two main channels – North Channel and South Channel (see Fig. 2). These two channels merge about 15 km from the mouth of the estuary. The South Channel is the main conduit for fresh water discharge through the estuary, while most of the tidal prism empties and fills through the North Channel. As a result the dynamics in the South and North Channel are very different. The daily tidal range may vary from less than 2 m during the neap tides to ~ 3.6 m during the spring tides. The tide is mixed, and predominantly semidiurnal with M_2 amplitude ~0.95 m and K_1 amplitude ~ 0.41 m at the lower estuary.

Columbia River has the second highest annual river discharge in the continental United States (second only to the Mississippi), resulting in a river-dominated estuary. River discharge shows considerable seasonal variability. Flows usually exceed 10,000 m^3s^{-1} during the spring freshet months (April-June) and may drop below 2,000 m^3s^{-1} during the dry season (July-October). This variability is, however, lower than the pre-dam period when discharges varied from 1,000 to 35,000 m^3s^{-1} (Bottom *et al.*, 2005). The highest flows in the Columbia River mainstem result from spring snow melt in the interior portion of the Columbia Basin, the lowest occur during very cold winter weather. The interior sub-basin

east of the Cascade mountains accounts for 91% of the surface area of the basin and ~75% of the flow. The Willamette River and other western tributaries account for the remaining 25% of the flow. Unlike the main stem, the highest flows in these tributaries are seen after winter rains, with floods occurring as the result of rain-on-snow events. Willamette flows form an appreciable part of the total discharge only from November through April.

Atmospheric forcing is also an important factor in the system. Broadly speaking, a typical year can be divided into three distinct periods. During the winter months from October to March, winds are strong and highly variable, but the strongest winds are from the south and southwest and lead to coastal downwelling. Winter river flows are variable; with the highest flows occurring during brief winter freshets and extreme low flows occurring during very cold periods. The spring freshet period from April to July is characterized by high river discharge. The spring transition from predominantly downwelling-favorable to predominantly upwelling-favorable wind conditions occurs during this season, usually in June. The summer–fall period from August to November has low to moderate discharge conditions and predominantly northerly winds (leading to upwelling in the coastal zone), typically until mid-October. Within each of these periods we observe characteristic neap-spring variations in response to tidal conditions and considerable variability in wind forcing.

3 Data and Data Processing

The multiple, interacting time scales that influence circulation of river-dominated estuaries precludes understanding the complete range of physical processes from short-term process studies alone. To provide insight into seasonal and inter annual processes, we rely here on observations from CORIE, an existing observatory designed to observe and predict the Columbia River ecosystem on a long-term basis (Baptista *et al*. 1999, Baptista 2006).

CORIE consists of two components – a real-time monitoring network and a numerical modeling system. The modeling system uses 3D circulation models (e.g., Zhang *et al.,* 2004) to produce daily forecasts and long-term retrospective simulation databases (Baptista *et al.,* 2005). The monitoring network, in place since 1996, consists currently (Baptista 2006) of instrumented stations at ~18 locations inside the estuary (Fig 2) and two offshore locations. CORIE instruments are predominantly of two types – inductive conductivity/temperature instruments (CTDs) that measure the salinity, temperature and

pressure at a single depth, and acoustic doppler profilers (ADPs) that measure the velocity profile above the instrument. The extensive temporal records from these stations allow studies of seasonal and interannual variability in ways that have not been possible in the Columbia River in the past.

CORIE Instrument Data

We focus here on data from the ADPs to resolve currents, and use the salinity data as a measure of transport processes. There are four ADPs in the estuary, at stations **am012**, **am169**, **red26** and **tansy** (Fig 2). Three of these stations (**am169**, **red26** and **tansy**) are located along the South Channel, and are therefore strongly influenced by river discharge. They are, however, located in different water depths. While **am169** (instrument depth = 18 m) is located near the center of the South Channel, **red26** (instrument depth = 16 m) is located close to the south edge of the South Channel in a reach where the strongest currents are on the south side of the channel. In contrast, **tansy** (instrument depth = 12 m) is south of the main channel, near the mouth of Youngs Bay, where river-bay tidal exchanges add to the complexity of the flow field. In the North Channel there is only one ADP station (**am012**, instrument depth = 20 m), located near the middle of the channel.

The ADPs record time series of velocity in vertical bins with a sampling time step that varies from 1 to 6 minutes. Vertical bins sizes depend on ADP frequency and vary from 0.25 m to 1 m. In each vertical bin, principal component analysis (Emery and Thomson, 2001) was used to define a coordinate system aligned with the principal axes (directions of maximum and minimum variance). Since the estuary channels are relatively narrow, the velocities along directions of maximum and minimum variance at all depths were essentially the along-channel and across-channel velocities, respectively. At all ADP stations, the across-channel velocity variance is less than 5% of the along-channel velocity variance. Consequently, all subsequent analyses in this paper have been carried out using the along-channel velocity component only. The most significant potential source of errors in the present ADP data set results from bio-fouling and consequent low signal to noise ratio (SNR) values. A considerable portion of the velocity data in 2002 and isolated sections from other years had to be discarded for this reason.

Salinity is determined algorithmically from the CTD sensors using the measured temperature and conductivity of a fixed control volume. Accurate salinity estimates can be obtained as long as the control

volume remains unchanged. However, small changes in this control volume can lead to significant errors in salinity estimates. Bio-fouling is the primary source of volume changes in these sensors. Unlike ADP sensors (where a significant amount of bio-fouling is needed to weaken the acoustic signal appreciably) even small amounts of bio-fouling can have a significant impact on CTD sensors. As a result, large segments of the salinity data were deemed unsuitable for our analyses.

External Data

Dynamical analyses require external forcing data (tides, river flow, atmospheric conditions) on appropriate time scales. Discharge from Bonneville dam, the most seaward of 13 mainstream dams, was obtained from a USGS gauge. Discharge data from a USGS gauge on the Willamette River (the main coastal tributary of the Columbia River) were used when available (Fig 2). Tidal information is obtained from a NOAA tidal gage located at Tongue Point (km-30, Fig 2). Wind data are determined from an offshore NOAA buoy (46029) located ~ 40 km west of the mouth of the Columbia River. In the following analyses we characterize the influence (both direct and indirect) of the different external forcings on circulation processes inside the estuary during different periods.

Filtering and Low-Frequency Data

A low-pass filter is used to separate the sub-tidal velocities (hereafter referred to as residual flow) and tidal velocities. The filter is defined in the frequency domain and is given by

$$\tilde{A}(f) = [0.5(1 - \tanh(30(f - f_c)))]A(f) \quad (1)$$

Where, $A(f)$ and $\tilde{A}(f)$ are the frequency-domain versions of the original and filtered signals, respectively, and f_c is the cut-off frequency for filtering. A hyperbolic tangent function is used to smooth cut-off.

To estimate the variation in the two-layer system, the residual inflow at each of the ADP stations was quantified using an “Inflow Number”, defined as:

$$\Omega_{in} = \frac{\sum_{j=1}^{N} \hat{u}_j \Delta z}{\sum_{j=1}^{N} |u_j| \Delta z} \quad (2)$$

Where, N is the total number of bins in the vertical direction, u_j is the residual velocity (positive values refer to flow moving into the estuary) in the j^{th} bin, and $\hat{u}_j$ is the residual inflow velocity given by

$$\begin{aligned} \hat{u}_j &= u_j \quad \text{for } (u_j > 0) \\ \hat{u}_j &= 0 \quad \text{for } (u_j < 0) \end{aligned} \quad (3)$$

Ω_{in} is a dimensionless, proportional inflow, with Ω_{in} = 0 for no inflow and Ω_{in} = 1 for complete inflow. A note of caution is needed regarding the interpretation of the Inflow Number. It is an indication of the *proportion* of total residual flow over the water column that is flowing into the estuary, not a measure of absolute residual inflow amplitude. Ω_{in} is especially useful for comparing stations with different depths and energy levels.

Tides Analysis methods

Tidal currents in the Columbia River estuary have diurnal, semidiurnal and overtide components, the latter from nonlinear interactions. For analysis of tidal processes, the time series of high-pass-filtered along-channel velocities were further resolved into their spectral components. Here, we focus on the diurnal and semidiurnal components only. The vertical structure of tidal currents is expected to be strongly influenced by changes in stratification and mixing associated with fluctuating river flow and winds, and the fortnightly tidal range variations, yielding non-stationary velocity amplitudes and phases. Thus, continuous wavelet transform (CWT) techniques were used to separate tidal data into their individual spectral components, because they provide information regarding the time evolution of frequency structure. CWT techniques have been successfully applied to oceanographic problems before (e.g. Shen *et al.,* 1994 for wind wave analysis, Panizzo *et al.,* 2002 for studies of land-slide generated waves, and Jay and Flinchem, 1997 and 1999 for tidal analysis).

The wavelet transform of a time series is formed by convolution of the time series with a set of wavelet

functions defined by a base (or mother) wavelet. The general transform is given by:

$$X_g[\tau,\alpha] = \frac{1}{\sqrt{\alpha}} \int_{-\infty}^{\infty} x(t) g^*_{\alpha\tau}(t) dt \quad (4)$$

Where, $x(t)$ is the data time series, τ is the translation parameter, α is the scale dilation parameter and $g_{\alpha\tau}(t)$ is a set of complex wavelet functions defined by $g_{\alpha\tau}(t) = g[\frac{(t-\tau)}{\alpha}]$, $g(x)$ being the base function. The choice of this base function is somewhat arbitrary, as long as certain properties are satisfied (see Meyers *et al.*, 1993 and Flinchem and Jay, 2000 for details) and is determined by the problem at hand. We have used a "Morlet wavelet" (Emery and Thomson, 2001) as our base function:

$$g(x) = e^{-x^2/2} e^{i\pi c x} \quad (5)$$

Where, c=2, so that the dilation parameter α in (4) corresponds to the period of the tidal component that we are trying to resolve. The function $X_g[\tau,\alpha]$ in (4) is a complex time series, representing the time-varying amplitude and phase of $x(t)$ at any given frequency.

One of the properties of wavelet transforms is that an increase in spectral resolution is accomplished at the cost of temporal resolution. To optimize temporal resolution, the analysis focuses on the diurnal (α = 1 day) and semidiurnal (α = 0.5 day) tidal species rather than on constituents (Flinchem and Jay, 2000). These species were resolved using filters of 61 and 121 hrs, respectively. Filters of this length are narrow enough to exclude non-tidal fluctuations while still resolving neap-spring transitions and related variations. Half a filter length of data is discarded at the beginning and end of the transform, to avoid end effects.

4 Results and Discussion

As stated in the introduction, we seek to describe the seasonal and inter-annual variations in tidal and sub-tidal circulation patterns, define how tidal processes affect residual flows and the salinity distribution, and document the response of tidal currents to the neap-spring cycle and seasonal variations in winds and river flow. To examine sub-tidal processes, we look at CORIE ADP data from April through December of 1997. These data are particularly valuable because they are relatively complete and cover a

large part of a year with the strongest spring freshet since 1974. Unfortunately most of the CTD sensors went into operation only in 2001, so salinity data were not available for this period in 1997.

4.1 Residual Flows

Prior studies (Hansen and Rattray, 1965; Jay and Musiak, 1996) suggest that the residual flow in the Columbia River is generated by two primary factors: a) mean horizontal density gradients, leading to gravitational circulation, and b) time-varying vertical mixing and stratification, leading to internal tidal asymmetry. Both of these factors, as well as the effects of atmospheric forcing, are evident in the four April to December of 1997 ADP time series of along-channel residual flow shown in Fig 3, though a lack of density structure data precludes a quantitative separation of the various processes.

The residual flow patterns show strong seasonal and tidal monthly variability. A two-layer residual pattern is observed at all stations, but is transient. The alternating establishment and breakdown of two-layer flow under neap and spring tidal conditions was reported by Jay and Smith (1990a). There are however distinctive residual flow patterns at the different stations. Residual inflow is the strongest in the North Channel station (**am012**) since it is the deepest station and least influenced by river discharge (Fain *et al*, 2000). In the South Channel, the strength of residual inflow is directly related to depth. After the spring freshet, the most upstream station (**am169)** records stronger residual inflow velocities than any other South Channel station because it lies in the main thalweg, where the density effects are expected to be the strongest. Both depth and inflow are intermediate at **red26**. The shallow depths at **tansy** limit the development of gravitational forcing. River outflow occurs throughout the water column during the spring freshet; inflow is weak for the remainder of the record.

Two other factors are of interest at **tansy**. The first factor is that landward flow, when it is re-established after the freshet, is not bottom concentrated, but appears at ~5-7 m depth. This leads to the suspicion that this landward flow is due to internal asymmetry (which may occur anywhere in the water column) rather than gravitational circulation, which increases toward the bed. The second factor is the rather strong neap-spring contrast in residual flow. Because **tansy** is on the outside of a channel bend, it is likely that the strong ebb currents during spring tides are displaced further to the south than is the case with the weaker ebbs during the neaps, leading to a stronger neap-spring contrast than for a straight channel. Stronger cross channel velocities (figure not shown) were observed at this station than at the

other stations (with the exception of **am012**). Additionally reduced salinity intrusion during spring tides may also reduce inflow.

The variation in Inflow Number Ω_{in} at the four ADP stations is shown in Fig 4, along with daily tidal range (from NOAA tidal gage), daily river discharge (from Bonneville dam) and daily averaged winds (at NOAA buoy 46029). During the spring freshet (May and June; flow >8,000 m^3s^{-1}), residual inflow is observed only at **am012** in the North Channel. The strong river outflow through the South Channel overcomes the baroclinic inflow and destroys the two-layer flow pattern at all other stations even during the weakest tides. This occurs despite flood salinity intrusion all the way to **am169** (Fig. 1). Comparing Ω_{in} for the South Channel (stations **am169**, **red26** and **tansy**) with the river flow and tides, we observe that when discharge is less than 8,000 m^3s^{-1} there is inflow is at all stations (Figs. 4-6). Ω_{in} peaks during the neap and decreases to 0 or near zero during the springs (Fig. 6). This breakdown of the two-layer residual flow during stronger tides occurs due to an increase in vertical mixing, which weakens the baroclinic flow into the estuary when a critical tidal range is reached (Jay and Smith, 1990b). This neap-spring transition, which occurs in the South Channel when river discharge falls below 8,000 m^3s^{-1} (approx) is clearly seen from a scatter diagram of Inflow Numbers vs river discharge (Fig. 5).

A similar feature is observed in the North Channel (station **am012**), but some inflow occurs on neap tides even for the highest flow levels observed (12,000 -14,000 m^3s^{-1}). Station **am012** differs from the three South Channel stations because of its greater depth and reduced influence of river discharge. Thus, $\Omega_{in} > 0$ in the North Channel during the weak tides, even under high discharge periods. In fact, as the river discharge falls below 8,000 m^3s^{-1} residual inflow is observed even during the large tides, and, in contrast to the observations in the South Channel stations, Ω_{in} actually increases during the larger tides (Fig. 6). The depth integrated residual inflow (computed by vertically integrating the inflow velocities) on the other hand continues to be stronger during the weaker tides (figure not shown here but shown for a different period in Fig. 7). This could be because enhanced tidal mixing reduces the salinity near the bottom but increases it near the surface. The residual inflow generated by the density gradients over the water column are strong enough to counteract the weak river outflow at this station, leading to a net residual inflow over a larger part of the water column and an increase in Ω_{in}, even though the total residual flow into the estuary is usually weaker than during the neap tides. Alternatively, cross channel advective

processes may play a strong role in the along channel velocity profiles as shown by the modeling and field studies of Lerczak and Geyer (2004) and Valle – Levinson *et al* (2000) respectively. Cross channel velocities at this station were found to be on the order of 0.1 ms^{-1} (figure not shown) which are strong enough to play an active role in the momentum balance of the along shore velocities. Furthermore, the cross channel velocities are distinctly stronger after the spring freshet. However, to explore this mechanism in further detail would require a detailed modeling and / or field study of the cross channel flow patterns which is not possible with a single instrument in the channel.

To compute a quantitative relation between the Inflow Number, river discharge and tidal range, we seek a solution of the form

$$\hat{\Omega}_{in} = a_0 Q^{N1} R^{N2} \tag{6}$$

Where, *Q* refers to the river discharge in 10^3 m^3s^{-1}, *R* the tidal range in m and a_0,*N1* and *N2* are the curve fitting parameters determined from the data. Fig. 6 shows the scatter diagram between Inflow Number and tidal range for the months of July and August, when river discharge and tidal range are the main forcing processes. The black dots indicate the actual data while the unfilled diamonds correspond to hindcast estimated values derived from solution of (6). The values of the parameters together with goodness of fit estimates (r^2) are also shown. A significant amount of the scatter in the data can be explained by the combined action of river discharge and tidal range.

As expected moreover, *N1* < 0 (Ω_{in} decreases with increased river flow) at all stations, and *N2* < 0 in the South Channel (Ω_{in} decreases with increased tidal range). |*N1*| and |*N2*| are smallest at **am012**, indicating that the North Channel is somewhat buffered from changes related to both flow and tidal range. This is consistent with its depth and remoteness for direct river discharge. The low value of |*N1*| at **red26** is similarly consistent with its seaward position. A relatively high value of |*N2*| at **am169** is consistent with the fact that this station is close to the upstream limit of salinity intrusion, which is quite sensitive to tidal range. Station **tansy** has the largest values of both |*N1*| and |*N2*|, whereas one would think that its |*N1*| values should be low due to its shallow depth, which reduces gravitational circulation. Strong cross channel velocities (in comparison to the other stations) indicate that large changes in residual flow at **tansy** due to tidal and river flow variability may be in part related to channel curvature and lateral

migration of circulation patterns, not just to changes in vertical mixing.

To summarize, the interaction between tides and river discharge lead to different patterns of residual flow in the two channels. In the South Channel, the classical two-layer residual flow pattern during neap cycles is seen only for low river discharge (below 8000 m^3s^{-1}) and disappears completely under high river discharge, even when and where salinity intrusion is still present. We deduce, therefore, that landward salt transport under high flow conditions occurs by tidal mechanisms. In the North Channel, a two-layer pattern is seen at neap tides during high river discharge, and at all times during the low river discharge. The total residual inflow in the North Channel is still inversely related to the tidal range (not shown) but Ω_{in} is larger during spring tides. The absence of density data for this time period precludes any quantitative assessment of the relative roles of gravitational circulation vs. internal asymmetry. However, the data at **tansy** suggest the presence of internal asymmetry, and Jay and Musiak (1994, 1996) have verified its presence at **am012** and **am169** for a variety of flow conditions, and tidal current patterns suggest its presence at all stations (as discussed below). Tidal mechanisms are likely, therefore, to be important in the salt transport, as they are at more seaward transects (Jay and Smith, 1990c; Kay et al. 1996)

Winds also play a role in the residual flow patterns of the Columbia River estuary. Fig. 4 shows that during a strong wind event in October (marked by the dotted vertical lines) the two layer residual flow patterns in the South Channel break down (indicated by a drop in the Inflow Number) even though the tides and river discharge are relatively weak. Winds can influence transport processes in several ways. One is the direct action of either wind-induced turbulence which would break down the two-layer residual flow pattern in a fashion similar to tidal mixing or the wind forcing itself which can setup secondary circulation cells (Winant, 2003). The second is a deepening of the offshore fresh water plume that can reduce the salt coming in to the estuary from the bottom and hence significantly reduce the baroclinic component of residual inflow. Finally, winds or pressure fluctuations can cause a barotropic surface slope change, which then leads to salt wedge displacement (barotropic adjustment) and a subsequent recovery (baroclinic adjustment) over a period of days. Jay and Smith (1990c) document such an occurrence in December 1981.

To explore the role of the different processes in reducing the residual inflow we need to look at salinity data, which was not available for this period. As a result we examine a different period with similar

conditions (high winds, low tides and river discharge) when both salinity and velocity data are available; we see similar phenomena. Fig. 7 shows the influence of winds and tides on the salinity and residual inflow from November 2001 through March 2002. Here, time series of the daily maximum salinities at two stations near the mouth of the estuary (**sandi** in the North Channel, and **red26** in the South Channel.; Fig. 2) were plotted together with the depth integrated residual inflow (at **am012**), and the external forcings (river discharge, tidal range, and winds). The CTD sensors at **sandi** and **red26** are in shallow water, close to the bottom (~1 m above the bottom) in depths of 7.6 and 9 m, respectively (the CTD and ADP sensors at **red26** are approximately 100 m apart, hence the difference in depths at the two sensors). These represent salinity propagation into the estuary near the mid-depth maximum in landward salt transport (Jay and Smith, 1990c; Kay and Jay, 1996). Because we are interested in total rather than proportional inflow, we use the depth-integrated residual inflow at **am012** instead of Ω_{in} to quantify the flow coming into the estuary. Note that in early November when winds and river discharge are both weak the residual inflow at **am012** is inversely related to the tides. This was stated but not explicitly shown earlier in the discussion of Fig. 6 on the response of the Inflow Number to tides in the North Channel. Also shown in Fig. 7 is a time series of sub-tidal elevation at the Tongue Point tide gauge, which reflects the strength of upwelling versus downwelling processes (sub-tidal elevation increases during downwelling), as well as time series of daily minimum salinities from a near surface sensor placed on an offshore buoy (**ogi01**, located approximately 25 km South West from the mouth of the estuary). Jay (1984) and Jay and Flinchem (1997) showed that mean elevation at Tongue Point responds primarily to coastal forcing rather than river flow, and the peaks in the elevation time series during periods of strong downwelling (marked by the dotted lines) in Fig. 7 bear this out.

From Fig. 7 we can discern three intervals (beginning of December 2001, middle of January 2002 and beginning of March 2002) when there is a consistent decreasing trend (on top of the shorter scale fluctuations) in maximum salinities near the bottom at **red26** and **sandi**. In all the cases the drop in salinities inside the estuary occur not during the periods of strong winds but some time after it, suggesting that wind induced mixing is not the direct cause of the reduction of salinity; wind forcing is, nonetheless, involved. In the first two events the drop in maximum salinities occurs when the winds change direction from downwelling to upwelling prevalent winds. Downwelling-favorable southerly winds deepen the low

salinity plume as well as move the plume to the north away from the mouth of the estuary. When the wind changes direction and the plume is pushed back south towards the mouth of the estuary the reduced offshore salinities propagate into the estuary, leading to a reduction in residual inflow (as seen in the data at **am012**). The movement of the plume back south is clearly seen in the time series of the daily minimum salinities from the surface CT sensor at **ogi01**, where there is a significant drop in the daily minimum salinities corresponding with a drop in the maximum salinities in the estuarine stations. Also note that from December 2001 through midway of January 2002 there are three distinct periods of downwelling persistent winds (marked by the dotted lines) followed by relaxation of winds, but that the reduction in estuarine salinity occurs only during the first and third case. Surface salinity data at **ogi01** shows that the wind relaxation after the second downwelling event was not significant enough to move the plume back in front of the estuary, thus signifying the importance of plume dynamics in salt propagation inside the estuary. Although consistent time-series data are not available during summer upwelling periods, vessel observations (not shown) indicate that upwelling brings water with S >33 into the estuary, reflecting the impact of coastal upwelling/downwelling on the estuarine exchange process.

To determine the direct impact of wind (along shore or across shore) on salinity we looked at salinity records at **am169** where CTD sensors were placed at different vertical levels. Fig. 8 shows the daily maximum salinities at these sensors for the same time period as Fig. 7. Salinity stratification (measured as the difference between the bottom and surface sensor data) together with the tides, winds and river flow have also been plotted. The near surface CTD sensor is more susceptible to small changes in river discharge as expected. The stratification data shows the expected neap – spring variability, particularly when the river discharge is below 4000 m^3s^{-1}. To isolate the impact of the individual forcing terms on stratification a regression analysis was done on the stratification data for a record extending from November 2001 to August 2004 (see Fig. 9). The impact of river discharge and tidal mixing can be clearly seen and a regression model similar to (6) accounts for most of the variation in the data (r^2 = 0.82). The data however does not show any correlation between stratification and the winds at this station, even after the discharge and tidal effects were removed from the data using the regression model (figure not shown). This suggests that the direct impact of winds on stratification is minimal in comparison to river flow and the tides. This however does not preclude an indirect impact of winds on salt transport and as will be shown

next there is empirical evidence to suggest that salt transport into the upper reaches of the estuary is suppressed during the winter months when the winds are stronger.

The effect of transitory residual inflow on the salt transport characteristics can be observed in the time series of an upstream CTD station (**eliot**). This station is located ~40 km upstream from the mouth of the Columbia River estuary, at a depth of 14.3 m (see Fig. 2); salinity intrusion occurs primarily during low-flow periods. Fig. 10 shows the daily maximum salinity at this station over 3 years together with forcing data. In general, salt is observed at **eliot** only during or just after neap tides, reflecting the stronger near-bed land-bed transport during periods of weak tides (Jay and Smith, 1990a). There are also two seasonal trends: 1) salinity intrusion decreases due to increased river discharge during spring freshets, and 2) a subtler tendency for salinity intrusion to decrease during the winter months when wind effects increase. This is discernible in the winter of 2001 (10/01 – 4/02) and 2003 (10/03 onwards) where salinity at **eliot** drops during the strong downwelling periods. The recovery in salinity during two neap tides in late December 2002 and early January of 2003 even under strong winds is most probably due to persistent downwelling conditions and consequent inability of the plume to move back towards the mouth of the estuary during periods of wind relaxation. Some of this is seen in the time series of daily minimum salinity at **ogi01**. Unfortunately this CORIE buoy was lost during a winter storm in December 2002 and the NOAA buoy compass also malfunctioned around this time (zero values for onshore wind velocities) which precludes us from confirming this hypothesis.

To summarize, residual flow fields in the Columbia River estuary show a strong influence of baroclinic processes and are sensitive not only to fluctuations in discharge, but also to alongshore winds (upwelling and downwelling) which changes the salinity of water intruding into the estuary. The net result of the interactions between these three factors is important because residual flow fields play a crucial role in transport characteristics in the upper reaches of the estuary. Due to the seasonal nature of river discharge patterns and shelf winds it is possible to qualitatively separate the influence of each individual external forcing. Seasonal features of salt transport are very well captured at both the offshore (**ogi01**) and upstream (**eliot**) gages. At the same time there is clear evidence of the coupling between the offshore and estuarine transport processes.

4.2 Tidal Circulation

It is useful, before discussing the interaction of tidal and non-tidal processes, to define the properties of tidal currents at the four ADP stations. Fig. 11 shows the semidiurnal velocity amplitudes as a function of depth and time for the four ADP stations, for the same time period as in Fig. 3. For comparison purposes, time series of semidiurnal elevation amplitude (obtained by performing a similar wavelet transform on the NOAA tidal gage data) together with the winds and the river flow have also been plotted. As expected, maximum current amplitudes generally coincide with maximum spring tides, and the velocity amplitudes at **tansy** are in general smaller than at the other stations because **tansy** is located in shallower waters outside the channel.

The vertical structure of semidiurnal velocity amplitude shows some differences between the two channels. In the South Channel, the maximum (in the vertical) velocity amplitudes are near the surface, and the amplitudes decrease near the bottom due to frictional effects. This is expected in a system dominated by barotropic processes. In the North Channel however, we observe that the maximum velocity amplitude is sometimes found lower in the water column. The disparity between the North and South Channels becomes clearer in a scatter diagram comparison between maximum (over depth) semidiurnal velocity amplitudes and corresponding tidal elevation amplitudes (Fig. 12). Both **red26** and **am169** show a relatively tight correlation between elevation amplitude and maximum velocity amplitudes. On the other hand, the correlations at **tansy** and **am012** are lower, especially **am012**. The lack of strong correlation at **tansy** may be related to channel curvature, because the station is located in shallower water outside of the salt wedge – as tidal range increases, it appears that the core of the flow moves to the south, closer to **tansy**. In contrast, the poor correlation between tidal forcing and maximum current amplitudes at **am012** is most probably due to baroclinic effects. Also, semidiurnal tidal amplitude at the Tongue Point gauge decreases with increasing flow due to a frictional bed stress interaction between tides and river flow (Kukulka and Jay, 2003), so some decrease in tidal current amplitude with increasing river flow may be expected, but this appears to be small seaward of Astoria.

Figure 13 shows the plots of diurnal tidal velocity amplitudes for the same time period. As in the semidiurnal flows, the peaks in velocity amplitudes for the diurnal flows generally coincide with corresponding peaks in tidal elevation amplitudes. The ratio of maximum diurnal current amplitude to

maximum diurnal height amplitude is near unity (taking **red26**, with the strongest currents, as an example). This is, perhaps surprisingly, very similar to the ratio of maximum semidiurnal current amplitude to maximum semidiurnal height amplitude at **red26**, whereas one would expect that the semidiurnal ratio would be about twice the diurnal ratio, because the semidiurnal wave (relative to the diurnal wave) must transport any given tidal prism in half the time. Jay and Musiak (1996) suggest a reason for this apparent anomaly: diurnal currents have a lower ratio of acceleration to friction, changing the wave number and wave length sufficiently to compensate for the difference in period. Nonetheless, both the maximum diurnal and semidiurnal waves have a clear relationship to tidal range.

The vertical structure of diurnal velocity amplitude, on the other hand, shows a fairly complex behavior. In the North Channel (**am012**), the maximum diurnal velocity amplitudes are located near the bottom with very small values at the surface, which is contrary to what we would expect for barotropic tidal flows. In the South Channel, the vertical structure varies between stations and over time. At **red26**, the maximum velocity amplitude shifts towards the bed during the high river discharge periods, while at **am169** the maximum velocity amplitude shifts towards the bed during the lower river discharge periods. The velocity flow field during spring freshets of 2002 and 1999 (figures not shown) indicates the same general trend, though not as clearly as during the larger spring freshet of 1997.

These features are related to tidal variations in salinity intrusion and vertical mixing, and the resulting, variable baroclinic contribution to tidal currents. Tidal propagation of salt into the estuary (and the subsequent development of horizontal density gradients) is controlled largely by the mean flow and semidiurnal tides. The diurnal tides render, however, tidal salinity intrusion asymmetric, with maximal asymmetry during peaks in diurnal tidal amplitudes. Consider the North Channel. During high flow periods, **am012** is near the head of salinity intrusion. Vessel observations described in Flinchem and Jay (2000) show that salt is totally removed from the vicinity of **am012** only on greater ebb. During the weaker ebb, vertical mixing processes are suppressed and there is incomplete removal of salt from the system, leading to strong density stratification and horizontal density gradients near the bottom. Near-bed velocities (opposed by the density gradients) are very low on weaker ebb, and there is a pronounced near-bed maximum on the following flood. Thus, diurnal fluctuations in the density field lead to diurnal fluctuations in velocity, and these are maximal near the bed at the leading edge of the salt wedge where horizontal

gradients are largest. At **am169** in the South Channel, strong, near-bed diurnal currents are seen only during low-moderate flow conditions, because salinity intrusion is minimal during high flows (see Fig. 1). Strong asymmetry is seen at **red26** primarily during high flows, because the salt front is rarely pushed back to **red26** under low-moderate flow conditions.

These phenomena can be seen more clearly from the profiles of along channel velocity on two different days – 19 June 1997 (Fig. 14) and 14 November 1997 (Fig. 15), when the river discharge are high (~ 15000 m^3s^{-1}) and moderate (~ 5000 m^3s^{-1}), respectively (see Fig. 4). In both figures, snapshots of velocity profiles are plotted for selected ebb and flood times of the two tides during the course of the day, as marked on a tidal time series. On 19 June 1997, we see that the velocity profiles during the strong flood event in Fig. 14 are vertically uniform at all the 4 stations, while during the weak flood event the vertical profiles show a maximum near the bottom at all the stations (except **am169**) due to the strong density gradients generated after the weak ebb. This feature is not observed at **am169** because the high river discharge during this period prevents the salt wedge from reaching this station except until just before high water. On 14 November 1997 (Fig. 15) on the other hand, the river discharge is around 5000 m^3s^{-1}, and increased velocities near the bottom during the "weak flood" is clearly discernible at all the stations. Higher velocities at the leading edge of the salt wedge (for the Fraser River) have also been reported by Geyer (1988). Since a significant component of the diurnal velocities are generated by interactions of the tide with a fluctuating density gradient (also referred to as internal tidal asymmetry in Jay and Musiak, 1996), the vertical structure of the tidal currents depend strongly on the location of the leading edge of the salt wedge. Since the salt wedge does not retreat past **am169** during low discharge and tidal conditions and rarely past **red26** for most weak tidal conditions (as seen in the maximum salinity data of near bed CTD sensors at these two stations in Figs. 7 and 8) the maximum velocity amplitudes are closer to the bottom at **red26** during the high discharge periods and closer to the bottom at **am169** during the low discharge periods. Thus, the interactions between salinity intrusion and river discharge strongly affect the vertical structure of diurnal velocity amplitudes in the South Channel.

To summarize, density gradients play a significant role in the vertical shear of diurnal tidal currents in both the channels. Semidiurnal flows in the North Channel show a nearly barotropic response, but internal tidal asymmetry plays a very dominant role in the generation of diurnal currents. Diurnal velocity

amplitudes in the South Channel show a seasonal trend associated with the movement of salt intrusion in response to river flow. The location of the intrusion front influences the local strength of vertical and horizontal density gradients differently at each station, causing time-space diversity and complexity in tidal current patterns. Winds do not seem to have any major discernible role on the velocity amplitudes of the tidal flows other than the retardation due to surface friction.

5 Conclusions

The two main channels in the Columbia River estuary have very distinctive dynamics. The South Channel has strong river outflow, moderate tidal currents and a less well-developed salt-wedge. The North Channel has weaker river outflow, more tidal transport, and a more salt-wedge like salinity intrusion. Thus, the two channels constitute, in effect, two rather different sub-estuaries, which increase both the complexity of the Columbia River circulation and the opportunity to observe a variety of dynamical conditions. Analyses of long time-series of moored ADP and CTD data have been carried out to a) characterize the variability in the flow field and corresponding transport processes of the Columbia River estuary under a variety of forcing conditions, b) understand the influence of tidal, fluvial and wind forcing on the low-frequency circulation, and c) define the influence of density forcing on the tidal flow. Our intention was to provide an understanding of the underlying processes in the circulation dynamics of the Columbia River estuary including the coupling with Shelf dynamics. The focus of the analyses was on ADP velocity time-series from four stations; analyses were carried out at the sub tidal (residual) and tidal time scales. Salinity data was used to qualitatively identify the exchange processes between the ocean and the river.

Residual velocities generally show a two–layer pattern with strong neap–spring variability and seasonal variability, the latter primarily due to river flow variations. In addition to seasonal and monthly fluctuations caused by variability in river discharge and tidal ranges, a reduction in residual inflow was also observed during periods of strong alongshore winds to the north. Apparently, shelf dynamics via downwelling and plume transport reduce the salinity of water flowing into the estuary on flood, which in turn leads to a reduction in the residual inflow. Stratification data shows a strong correlation with river flow and tidal range but minimal correlation with the winds. However, winds, river flow, and tidal range all influence the position of the landward limit of salt intrusion, and the strongest salinity intrusion occurs, not

during periods of greatest tidal ranges, but during periods of highest residual inflow, as influenced by all three factors.

Tidal and subtidal fluctuations in horizontal and vertical density gradients and consequent tidal variations mixing also play a critical role in velocities at the tidal scale. Non-stationarity of the tidal flow has been studied by extracting semidiurnal and diurnal species using continuous wavelet transforms. As expected, peaks in velocity amplitude coincide with peaks in tidal elevation amplitude for both the diurnal and semidiurnal tidal species. The vertical structures of velocity amplitude however show considerable variability. Semidiurnal velocity amplitudes in the South Channel follow the same trends expected of barotropic processes and show limited sensitivity to salt wedge dynamics. In the North Channel however, semidiurnal velocity amplitudes show variability in their vertical profile and though the exact mechanism for this variability is not clear yet, the salt wedge position is suspected to play a significant role. Diurnal velocities in both the South and North Channel are strongly influenced by salt wedge position, and the South Channel flows show greater variations due to stronger seasonal trends in the moving salt wedge. Thus, there is strong coupling between the residual (which positions the salinity intrusion) and tidal flows in the Columbia River estuary.

The complex seasonal and monthly circulation patterns that we have observed in the data highlight the crucial role played by the tides, river outflow and shelf winds. Table 1 summarizes the response of estuarine circulation to the different forcings. This study also showcases the importance of coastal observatories in understanding the physical processes in a highly dynamic system such as the Columbia River system. A permanent network of observation stations allow us to explore long term variability and at the same time identify interesting events (such as the reduction in salt intrusion due to downwelling) that can then be explored in greater detail.

Acknowledgments ADP and CTD data for this project came from CORIE, co-author Baptista's prototype coastal-margin observation and prediction system for the Columbia River and adjacent coast. The National Oceanic and Atmospheric Administration (AB133F-04-CN-0033), U.S. Fish and Wildlife Service (133101J104) and the National Science Foundation (ACI-0121475 and OCE-0239072) provided financial support for this research and for the development of CORIE. We are also grateful to the

Bonneville Power Administration, National Oceanic and Atmospheric Administration, U.S. Geological Survey and U.S. Army Corps of Engineers for providing additional data. We thank Philip M. Orton of Lamont-Doherty Earth Observatory (Columbia University) for plotting the along channel density sections shown in Fig. 1. Any statements, opinions, findings, conclusions or recommendations expressed in this material are those of the authors and do not necessarily reflect the views or policies of the federal sponsors, and no official endorsement should be inferred.

References

Burla M., Baptista, A. M., Casillas, E., and Williams, J. G. "The influence of the Columbia River plume on the survival of steelhead (Oncorhynchus mykiss) and chinook salmon (O. tshawytscha): a numerical exploration", submitted December 2006 to *Canadian Journal of Fisheries and Aquatic Sciences*

Baptista, A. M. (2006) "CORIE: the first decade of a coastal-margin collaborative observatory", *Oceans'06*, MTS/ IEEE, Boston, MA

Baptista, A. M., Wilkin, M., Pearson, P., Turner, P., McCandlish C., and Barrett, P. (1999) "Coastal and estuarine forecast systems – A multi-purpose infrastructure for the Columbia River", *Earth System Monitor,* **9**(3).

Baptista, A. M., Zhang, Y., Chawla, A., Zulauf, M., Seaton, C., Myers E. P. III, Kindle, J., Wilkin, M., Burla, M., and Turner, P. J. (2005) "A cross-scale model for 3D baroclinic circulation in estuary-plume-shelf systems: II. Application to the Columbia River", *Continental Shelf Research*, **25**, 935 – 972.

Bottom, D. L., Simenstad, C. A., Burke, J., Baptista, A. M., Jay, D. A., Jones, K. K., Casillas, E., and Schiewe, M. H. (2005) "Salmon at river's end: The role of the estuary in the decline and recovery of Columbia River salmon", *U.S. Dept. of Commerce, NOAA Tech. Memo.*, NMFS-NWFSC-68, 246 p.

Davies, A. M. (1990) "On the importance of time varying eddy viscosity in generating higher tidal harmonics", *Journal of Geophysical Research*, **95**(C11), 20287–20312.

Davies, A. M. (1993) "Numerical problems in simulating tidal flows with a frictional-velocity-dependent eddy viscosity and the influence of stratification", *International Journal for numerical methods in fluids*, **16**, 105–131.

Emery, W. J., and Thomson, R. E. (2001) *Data Analysis Methods in Physical Oceanography*, chapter Wavelet Analysis, pages 501–505. Elsevier, second edition.

Fain, A. M. V., Jay, D. A., Wilson, D. J., Orton, P. M., and Baptista, A. M. (2001) "Seasonal, monthly and tidal patterns of particulate matter dynamics in the Columbia River estuary", *Estuaries*, **24**, 770-786.

Flinchem, E. P., and Jay, D. A. (2000) "An introduction to wavelet transform tidal analysis methods", *Estuarine, Coastal and Shelf Science*, **51**, 177–200.

Geyer, W. R. (1988) "The advance of a salt wedge: observations and dynamical model", In J. Dronkers and W. van Leussen, editors, *Physical Processes in Estuaries*, pages 181–195. Springer-Verlag, New York.

Hansen, D. V., and Rattray, M. J. (1965) "Gravitational circulation in straits and estuaries", *Journal of Marine Res.*, **23**, 104–122.

Ianniello, J. P. (1977) "Tidally induced residual currents in estuaries of constant breadth and

depth", *Journal of Marine Res.*, **35**(4), 755–786.

Jay, D. A., and Flinchem, E. P. (1997) "Interaction of fluctuating river flow with a barotropic tide: A demonstration of wavelet tidal analysis methods", *Journal of Geophysical Research*, **102**(C3), 5705–5720.

Jay, D. A. (1984), *Circulatory processes in the Columbia River Estuary*, CREST, Astoria, Oregon, 169 pp. plus appendices.

Jay, D. A., and Flinchem, E. P. (1999) "A comparison of methods for analysis of tidal records containing multi-scale non-tidal background energy", *Continental Shelf Research*, **19**, 1695–1732.

Jay, D. A., and Musiak, J. D. (1996) "Internal tide asymmetry", In C. B. Pattiaratchi, editor, *Mixing in Estuaries and Coastal Seas*, Coastal and Estuarine Studies, pages 211–249, American Geophysical Union, Washington D.C.

Jay, D. A., and Smith, J. D. (1990a) "Circulation, density distribution and neap-spring transitions in the Columbia River estuary", *Progress in Oceanography*, **25**, 81–112.

Jay, D. A., and Smith, J. D. (1990b) "Residual circulation in shallow estuaries: I. Highly stratified, narrow estuaries", *Journal of Geophysical Research*, **95**, 711–731.

Jay, D. A., and Smith, J. D. (1990c) "Residual circulation in shallow estuaries:2. Weakly stratified and partially mixed, narrow estuaries", *Journal of Geophysical Research*, **95**, 733–748.

Kay, D. J., Jay, D. A., and Musiak, J. D. (1996) "Salt transport through an estuarine cross-section calculated from moving vessel ADCP and CTD data", *Buoyancy Effects on Coastal and Estuarine Dynamics*, AGU Coastal and Estuarine Studies **53**:195-212.

Kay, D. J., and Jay, D.A. (2003) "Interfacial mixing in a highly stratified estuary 2. A "method of constrained differences" approach for the determination of the momentum and mass balances and the energy of mixing", *Journal of Geophysical Research,* **108**(C3),18-1 – 18-11.

Kukulka, T., and Jay, D. A. (2003a) "Impacts of Columbia River discharge on salmonid habitat I. a non-stationary fluvial tide model", *Journal of Geophysical Research*, **108**, 3293 doi 10.1029/2002JC001382.

Lerczak. J. A., and Geyer, W. R. (2004) "Modeling the lateral circulation in straight, stratified estuaries", *Journal of Physical Oceanography*, **34**, 1410 – 1428.

Li, C., and O'Donnell, J. (1997) "Tidally driven residual circulation in shallow estuaries with lateral depth variation", *Journal of Geophysical Research*, **102**(C13), 27915–27929.

McCarthy, R. K. (1993) "Residual currents in tidally dominated, well-mixed estuaries", *Tellus*, **45A**, 325–340.

Meyers, S. D., Kelley, B. G., and O'Brien, J. J. (1993) "An introduction to wavelet analysis in oceanography and meteorology: With application to the dispersion of the yanai waves", *Monthly Weather Review*, **121**, 2858–2866.

Monismith, S. G., and Fong, D. A. (1996) "A simple model of mixing in stratified tidal flows", *Journal of Geophysical Research*, **101**, 28583 – 28597.

Panizzo, A., Bellotti, G., and Girolamo, P. D. (2002) "Application of wavelet transform analysis to landslide generated waves", *Coastal Engineering*, **44**, 321–338.

Shen, Z., Wang, W., and Mei, L. (1994) "Fine structure of wind waves analyzed with wavelet transforms", *Journal of Physical Oceanography*, **24**, 1085–1094.

Sherwood, C., Jay, D. A., Harvey, R., Hamilton, P., and Simenstad, C. (1990) "Historical changes in the Columbia River estuary", *Progress in Oceanography*, **25**, 299–352.

Simpson, J. H., Brown, J., Matthews, J., and Allen, G. (1990) “Tidal straining, density currents and stirring in the control of estuarine stratification”, *Estuaries*, **13**(2), 125–132.

Sontex (1997) *SonTex ADP Acoustic Doppler Profiler Technical Manual*. SONTEX, San Diego CA. version 4.4.

Uncles, R. J., and Stephens, J. A. (1990) “The structure of vertical current profiles in a macro tidal, partly-mixed estuary”, *Estuaries*, **13**(4), 349–361.

Valle-Levinson, A., Wong, K.-C., and Lwiza, K. M. M. (2000) “Fortnightly variability in the transverse dynamics of a coastal plain estuary”, *Journal of Geophysical Research*, **105(C2)**, 3413 – 3424.

Winant, C. D. (2004) “Three-dimensional wind-driven flow in an elongated, rotating basin”, *Journal of Physical Oceanography*, **34**, 462 – 476.

Zhang, Y. L., Baptista, A. M., and Myers, E. P. III (2004) “A cross-scale model for 3D baroclinic circulation in estuary-plume-shelf systems: I. formulation and skill assessment”, *Continental Shelf Research*, **24**, 2187 – 2214.

Table 1: Summary of the influence of external forcings on circulation dynamics at various scales inside the Columbia River estuary

	External Forcing		
Scale	Winds	Discharge	Tides
Residual circulation	Influence on baroclinic forcing through exchange dynamics with the Shelf	A dominant seasonal influence (due to spring freshets)	A dominant neap spring influence (due to tidal asymmetry)
Semidiurnal circulation	Negligible influence	Modest influence due to frictional bed stress interactions	A dominant barotropic influence, with a weak baroclinic influence of tidal asymmetry in the North Channel
Diurnal circulation	Negligible influence	A moderate influence in the South Channel (due to impact of moving salt wedge on tidal asymmetry)	A dominant baroclinic influence (tidal asymmetry)

Table 2: Summary of CORIE data used in the development of process based benchmarks

Station ID	Instrument type	Data type	Period covered (m/d/y)
am012	ADP	Velocity	05/22/1997 – 11/30/1997
			07/28/2001 – 04/23/2002
am169	ADP	Velocity	04/01/1997 – 11/30/1997
	CTD	Salinity	11/09/2001 – 08/05/2004
tansy	ADP	Velocity	03/25/1997 – 11/30/1997
red26	ADP	Velocity	04/21/1997 – 11/30/1997
	CTD	Salinity	10/30/2001 – 05/16/2002
sandi	CTD	Salinity	10/30/2001 – 05/16/2002
eliot	CTD	Salinity	08/31/2001 – 03/10/2004
ogi01	CTD	Salinity	08/31/2001 – 12/14/2002

Figure Captions

Fig. 1: Salinity intrusion (developed from vessel CTD cast data) in the South Channel of the Columbia River estuary (see map in Fig. 2) during two very different spring freshet periods, 1997 and 2001. These correspond to the highest and lowest spring freshets respectively, of the last decade. Salt intrusion doubles with a decrease in river flow by a factor of four; distance is measured along the South Channel from the mouth of the estuary. Bonneville flow refers to river discharge. The x axis is in longitudes along the channel. To compare with the map in Fig. 2 the longitudes of select locations are provided: Mouth of the estuary (-124.08), station **red26** (-123.95), station **tansy** (-123.92), station **am169** (-123.85), NOAA tidal gage (-123.767).

Fig. 2: Columbia River estuary shoreline and bathymetry. Bathymetry contours are in metres and are based on the NGVD29 vertical datum. The 4m contour is indicated by a light grey line and is used to distinguish between the tidal flats and the channels inside the estuary. A subset of CORIE observation stations that have been used in this analysis are shown. Also shown are the NOAA buoy 46029 (for offshore wind conditions) and NOAA tidal station at Tongue Point (Astoria).

Fig. 3: Along channel residual velocities (in ms^{-1}) as a function of time and depth for the four ADP stations during 1997. Positive velocities are landward. The vertical axis (z) is positive upward and refers to the distance (in m) from the mean sea level (MSL). The contours for **am012**, **am169** and **red26** extend from -0.5 ms^{-1} to 0.5 ms^{-1} with an interval of 0.1 ms^{-1} and the contours for **tansy** extend from -0.25 ms^{-1} to 0.25 ms^{-1} with an interval of 0.05 ms^{-1}

Fig. 4: Time series of dimensionless Inflow Number for the four ADP stations, daily tidal range (NOAA tidal gage), daily averaged along and onshore winds (NOAA buoy; +ve values refer to winds blowing from the south and west respectively) and daily averaged river discharge (Bonneville dam).

Fig. 5: Inflow Number vs River Discharge for the four ADP stations. The North Channel station (am012) shows consistently a double layer flow. For the South Channel stations, a transition occurs around river discharge 8,000 m^3s^{-1}, above which no two layer pattern develops.

Fig. 6: Inflow Number vs Tidal Range for ADP data between July and August in Fig. 4. Filled circles corresponds to actual data and open diamonds corresponds to curve fitting.

Fig. 7: Time series of daily maximum salinity at two estuarine stations (**sandi**; instrument depth =7.9 m and **red26**; instrument depth=9m), daily minimum salinity at **ogi01** (instrument depth=1m), the depth integrated residual inflow (at **am012**), the daily tidal range, the daily averaged along shore (positive values refer to downwelling conditions) and across shore winds, the sub tidal elevation, and the daily river flow. Time is in months for the years 2001/2002.

Fig. 8: Time series of daily maximum salinity at 2 different vertical positions at **am169**. Also plotted are the corresponding stratification (salinity difference between the bottom and top sensor), tidal range, along shore wind component, across shore wind component, wind speed and the daily river flow. The time series covers the same period as in Fig. 7.

Fig. 9: Scatter plots of stratification data (dots) as a function of river discharge, tidal range, along shore and across shore winds. A regression model (squares) similar to eqn. (6) was developed for the data with the following parameter values – a_0 = 16.45, $N1$ = 0.65, $N2$ = -1.39, r^2 = 0.82 and accounts for a significant part of the variation in the stratification data. Scatter plots are from time series extending from November 2001 to August 2004.

Fig. 10: Time series of daily maximum salinity (**eliot**; instrument depth=13.6 m), daily minimum salinity (**ogi01**; instrument depth=1m) along with tidal range, alongshore and onshore wind components, sub-tidal elevation and river discharge. Time is in MM/YY format and the time series extends from September 2001 through March 2004.

Fig. 11: Semidiurnal tidal velocity amplitude (in ms^{-1}) as a function of depth and time at all four ADP stations. Velocity amplitude contours extend from 0 ms^{-1} to 1.5 ms^{-1} with an interval of 0.25 ms^{-1}. The period of time covered is the same as in Figs. 3 and 4. Also shown are time series of semidiurnal tidal elevation amplitude (in m), and the daily averaged winds and river discharge.

Fig. 12: Scatter plots of maximum (over depth) semidiurnal velocity amplitude (y-axis) vs semidiurnal tidal

elevation amplitude (x-axis) at the four ADP stations. Goodness of fit parameter (r^2) as well as the slope (m) and intercept (c) are also shown.

Fig. 13: Diurnal tidal velocity amplitude (in ms^{-1}) as a function of depth and time at the four ADP stations. Velocity amplitude contours extend from 0 ms^{-1} to 0.5 ms^{-1} with an interval of 0.1 ms^{-1}. The time period is the same as in Figs. 3, 4 and 11. Also shown are time series of diurnal tidal elevation amplitude (in m) and the daily averaged winds and river discharge.

Fig. 14: Along channel velocity profiles at the four ADP stations for two tidal periods on 06/19/1997; river flow is ~15000 m^3s^{-1} (see Fig. 4). Instances of vertical profiles are marked on a tidal time series. Time is in hours and extends from 6/19/1997 0600 hrs to 6/20/1997 0600 hrs.

Fig. 15: Along channel velocity profiles at the four ADP stations for two tidal periods on 11/14/1997; river flow is ~5000 m^3s^{-1}; details as in Fig. 14. Time series now extends from 11/14/1997 1800 hrs to 11/15/1997 1800 hrs.

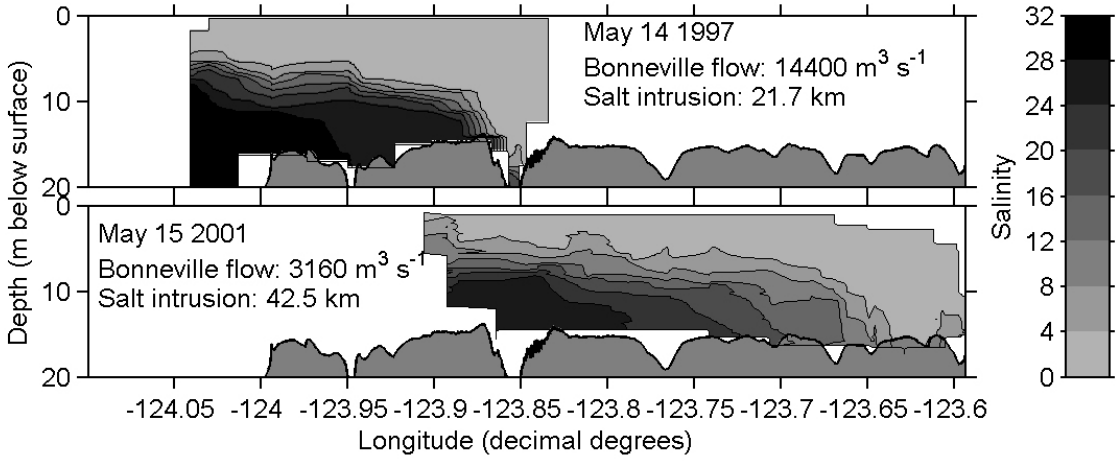
May 14 1997
Bonneville flow: 14400 m3 s-1
Salt intrusion: 21.7 km
May 15 2001
Bonneville flow: 3160 m3 s-1
Salt intrusion: 42.5 km
Depth (m below surface)
0
10
20
-124.05 -124 -123.95 -123.9 -123.85 -123.8 -123.75 -123.7 -123.65 -123.6
Longitude (decimal degrees)
Salinity
32
28
24
20
16
12
8
4
0

Figure 1

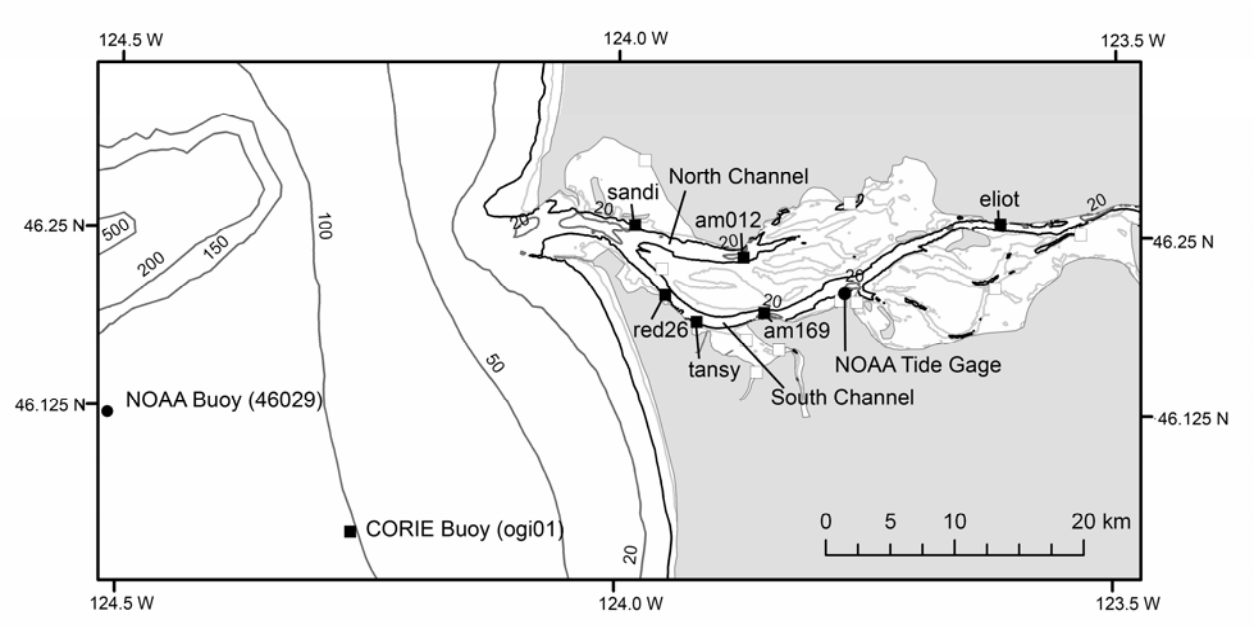
124.5 W
124.0 W
123.5 W
46.25 N
46.125 N
500
200
150
100
50
20
NOAA Buoy (46029)
CORIE Buoy (ogi01)
North Channel
sandi
am012
eliot
red26
tansy
am169
South Channel
NOAA Tide Gage
0 5 10 20 km

Figure 2

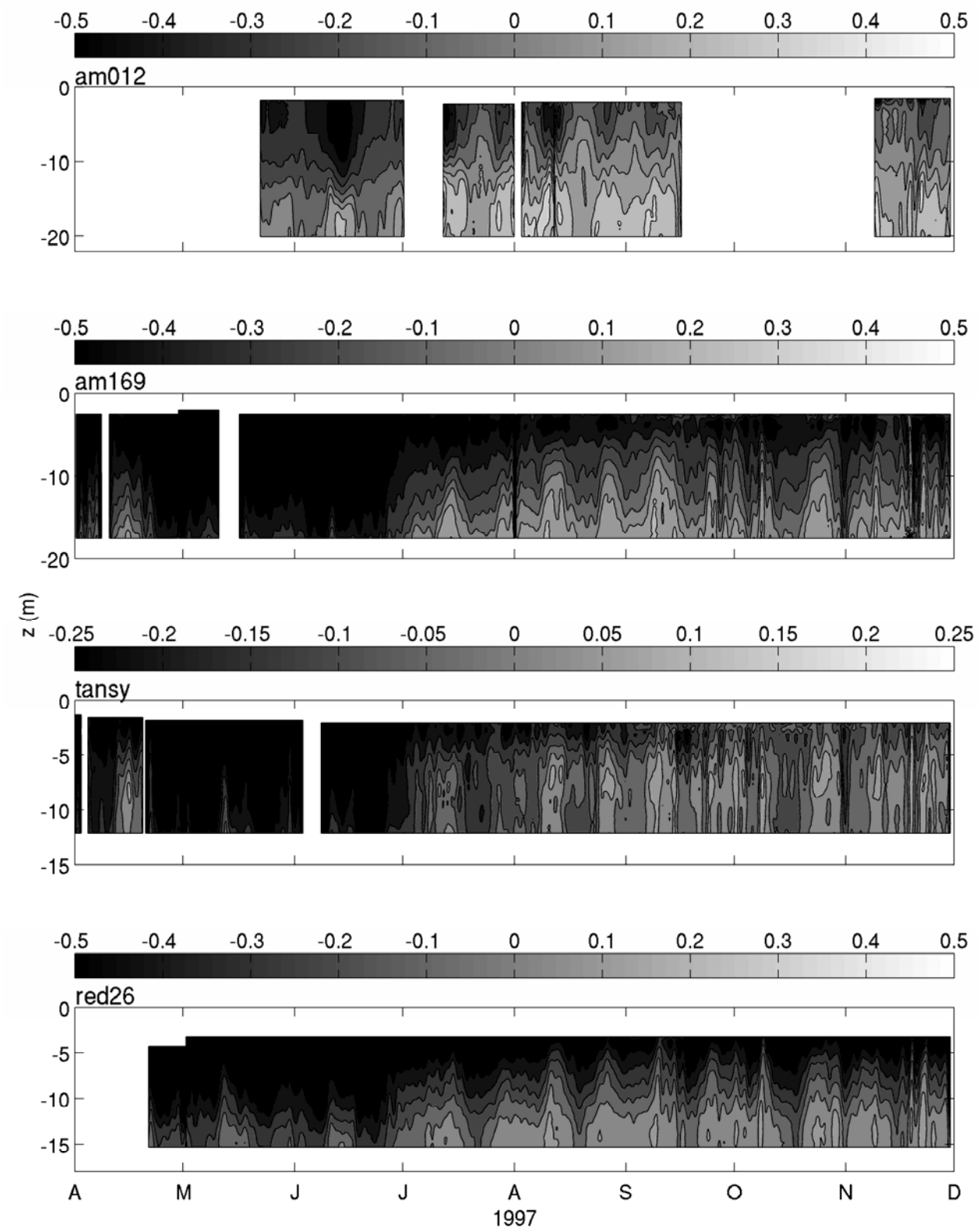
-0.5 -0.4 -0.3 -0.2 -0.1 0 0.1 0.2 0.3 0.4 0.5
am012
0
-10
-20
-0.5 -0.4 -0.3 -0.2 -0.1 0 0.1 0.2 0.3 0.4 0.5
am169
0
-10
-20
z (m)
-0.25 -0.2 -0.15 -0.1 -0.05 0 0.05 0.1 0.15 0.2 0.25
tansy
0
-5
-10
-15
-0.5 -0.4 -0.3 -0.2 -0.1 0 0.1 0.2 0.3 0.4 0.5
red26
0
-5
-10
-15
A M J J A S O N D
1997

Figure 3

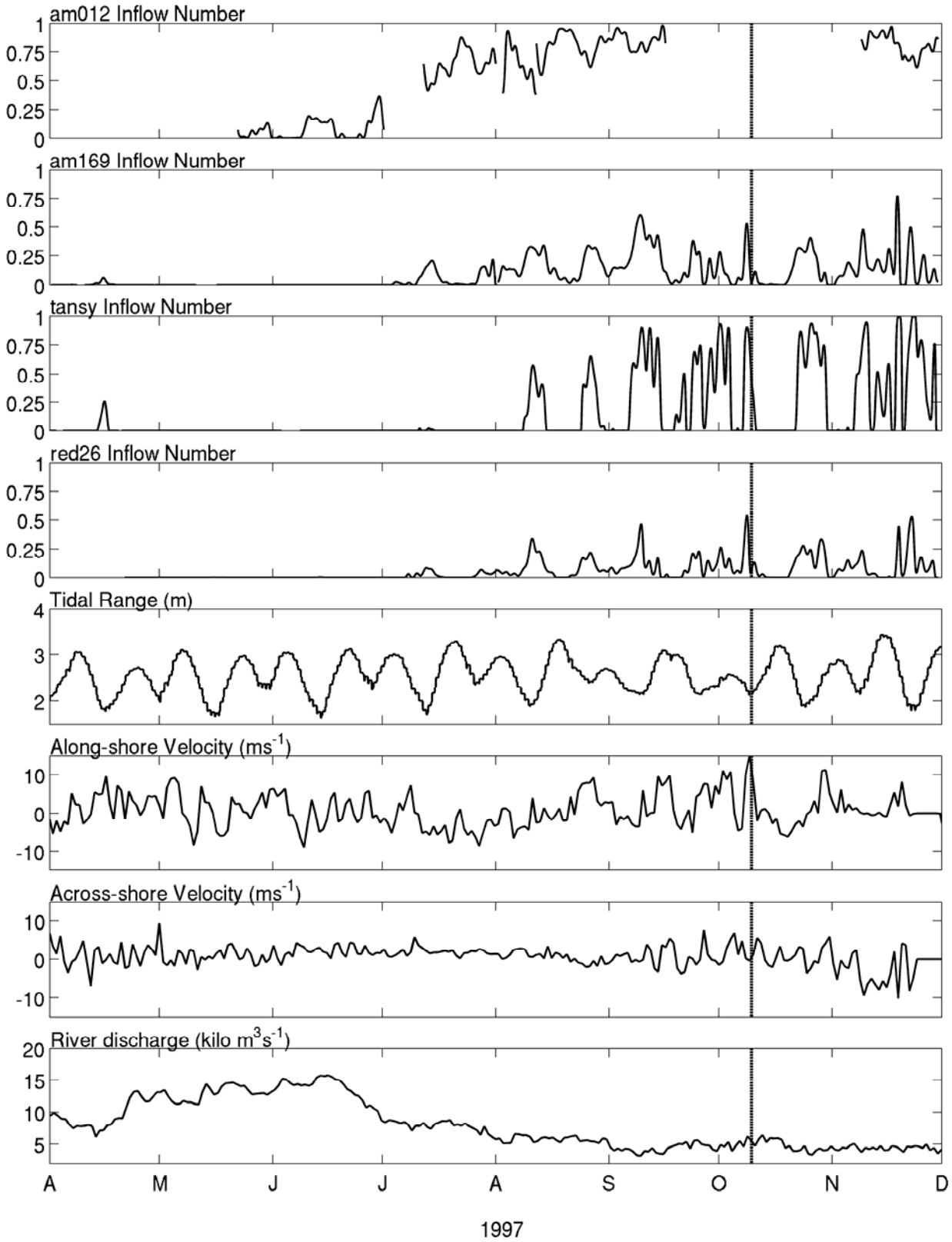
am012 Inflow Number
1
0.75
0.5
0.25
0
am169 Inflow Number
1
0.75
0.5
0.25
0
tansy Inflow Number
1
0.75
0.5
0.25
0
red26 Inflow Number
1
0.75
0.5
0.25
0
Tidal Range (m)
4
3
2
Along-shore Velocity (ms-1)
10
0
-10
Across-shore Velocity (ms-1)
10
0
-10
River discharge (kilo m3s-1)
20
15
10
5
A
M
J
J
A
S
O
N
D
1997

Figure 4

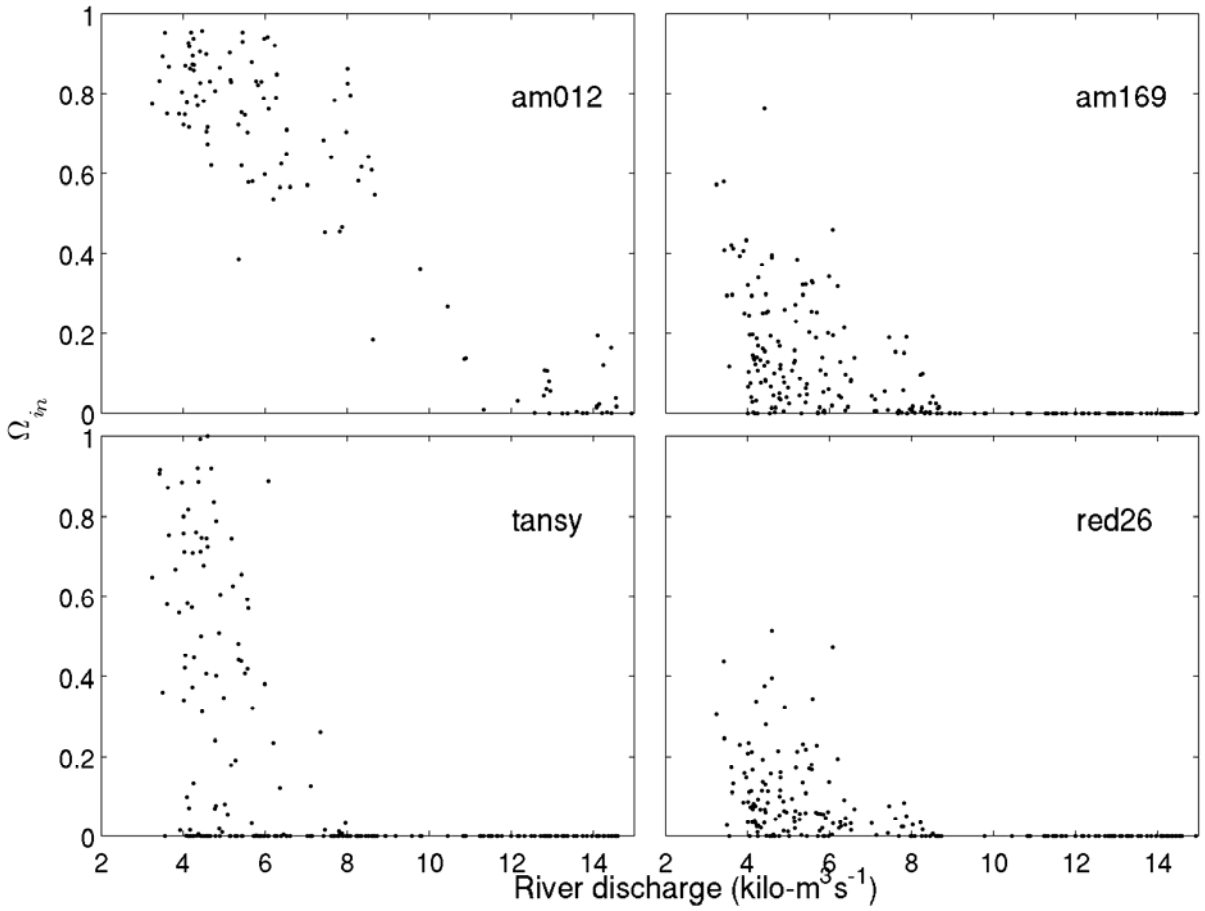

Figure 5

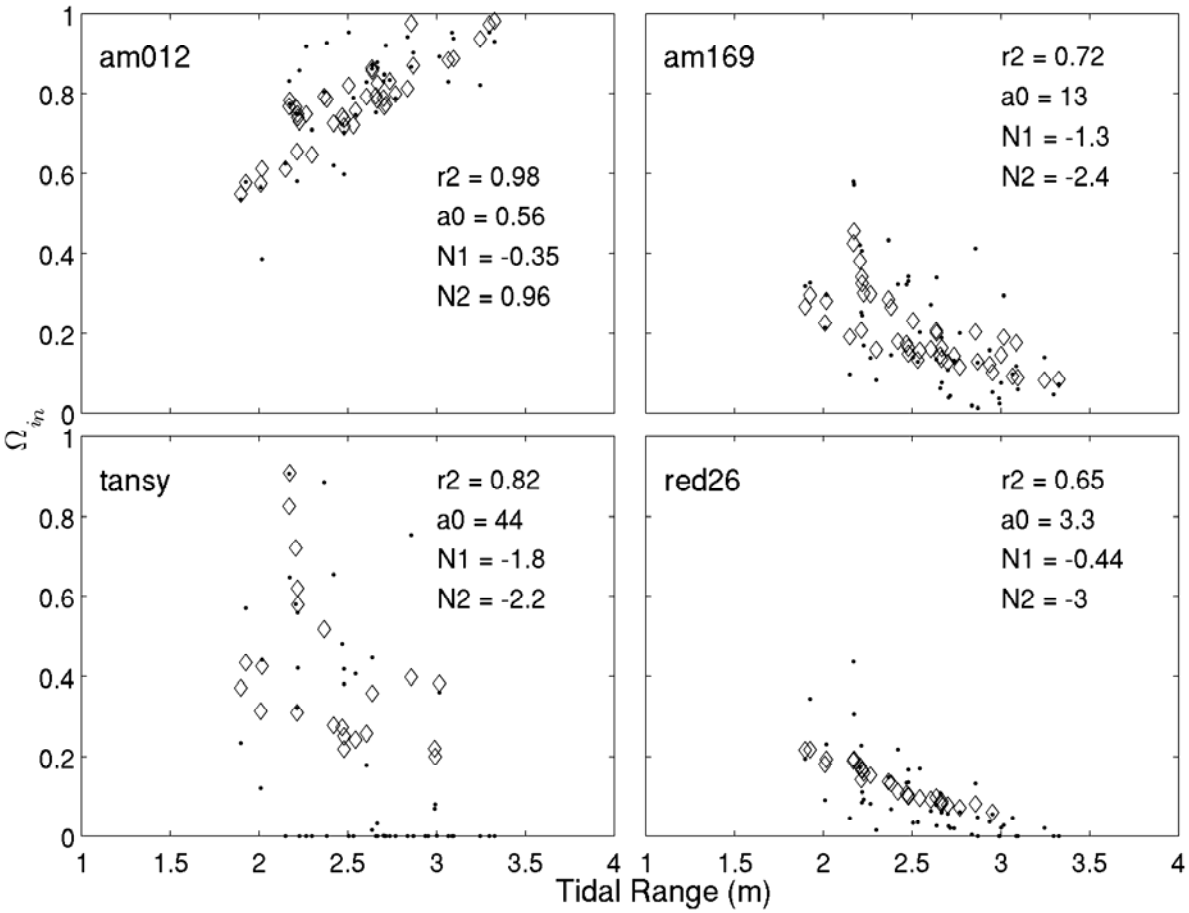
am012
r2 = 0.98
a0 = 0.56
N1 = -0.35
N2 = 0.96
am169
r2 = 0.72
a0 = 13
N1 = -1.3
N2 = -2.4
tansy
r2 = 0.82
a0 = 44
N1 = -1.8
N2 = -2.2
red26
r2 = 0.65
a0 = 3.3
N1 = -0.44
N2 = -3
Ω_{in}
Tidal Range (m)

Figure 6

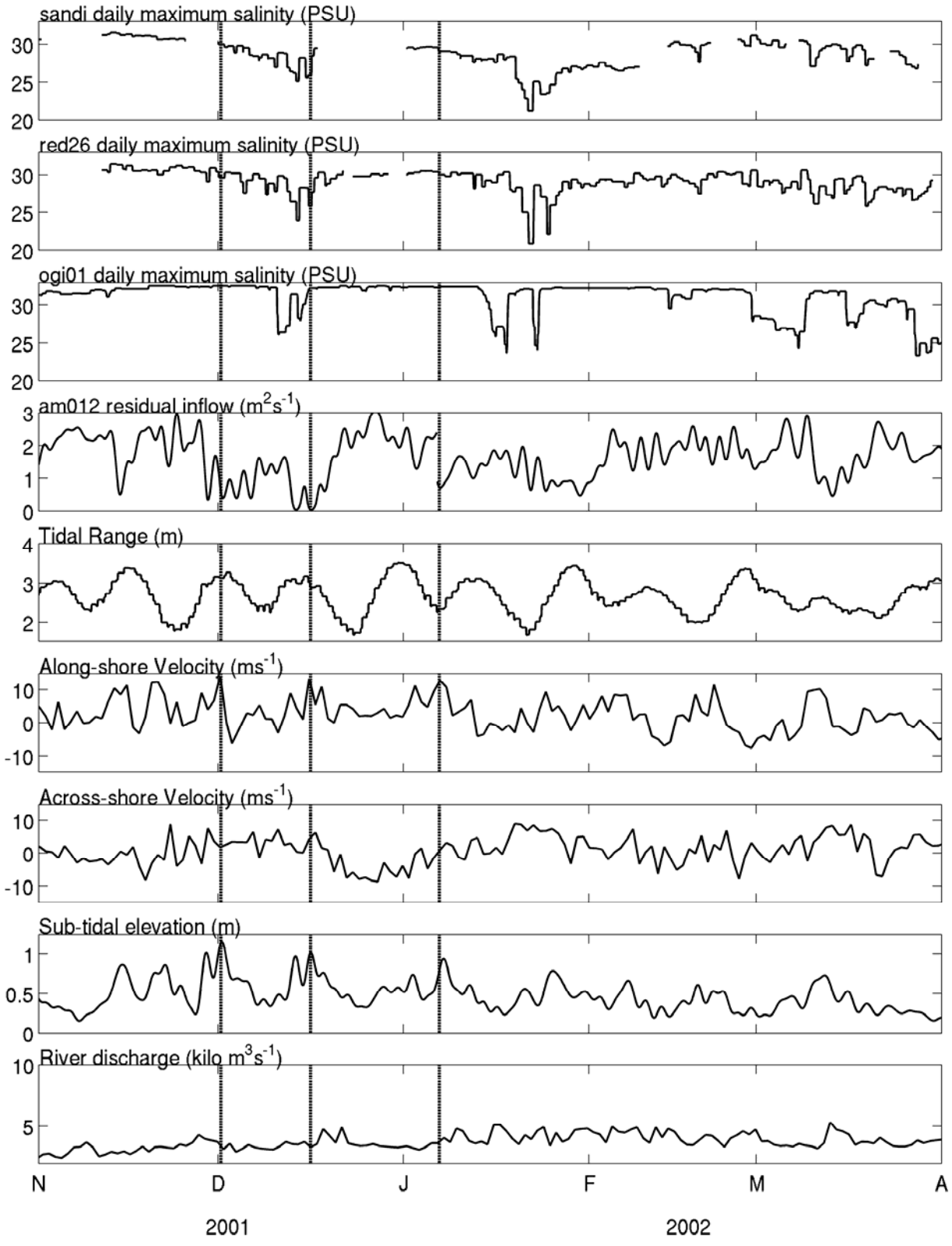
sandi daily maximum salinity (PSU)
red26 daily maximum salinity (PSU)
ogi01 daily maximum salinity (PSU)
am012 residual inflow (m2s-1)
Tidal Range (m)
Along-shore Velocity (ms-1)
Across-shore Velocity (ms-1)
Sub-tidal elevation (m)
River discharge (kilo m3s-1)
N
D
J
F
M
A
2001
2002

Figure 7

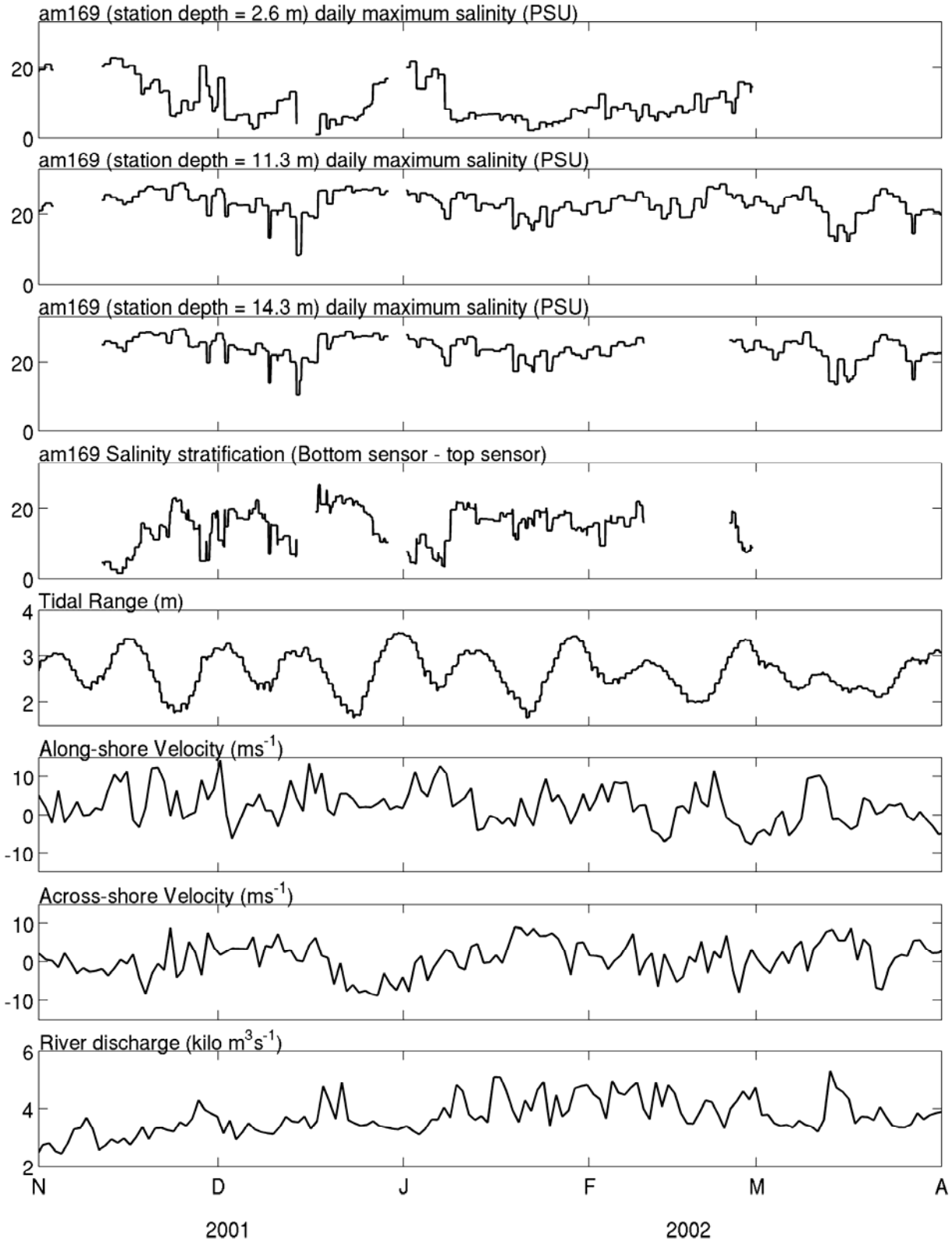
am169 (station depth = 2.6 m) daily maximum salinity (PSU)
20
0
am169 (station depth = 11.3 m) daily maximum salinity (PSU)
20
0
am169 (station depth = 14.3 m) daily maximum salinity (PSU)
20
0
am169 Salinity stratification (Bottom sensor - top sensor)
20
0
Tidal Range (m)
4
3
2
Along-shore Velocity (ms-1)
10
0
-10
Across-shore Velocity (ms-1)
10
0
-10
River discharge (kilo m3s-1)
6
4
2
N
D
J
F
M
A
2001
2002

Figure 8

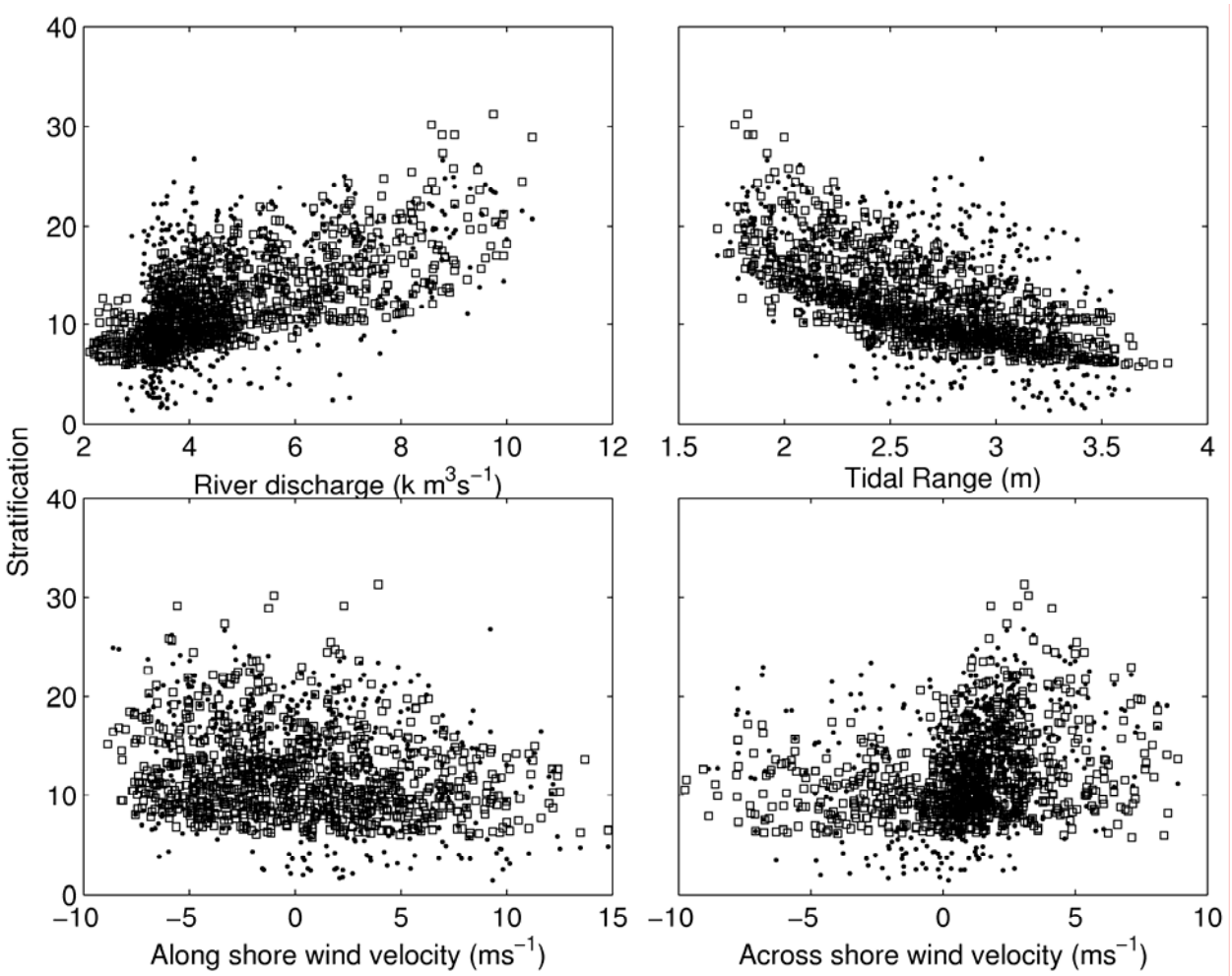
Stratification
River discharge (k m^{3}s^{-1})
Tidal Range (m)
Along shore wind velocity (ms^{-1})
Across shore wind velocity (ms^{-1})

Figure 9

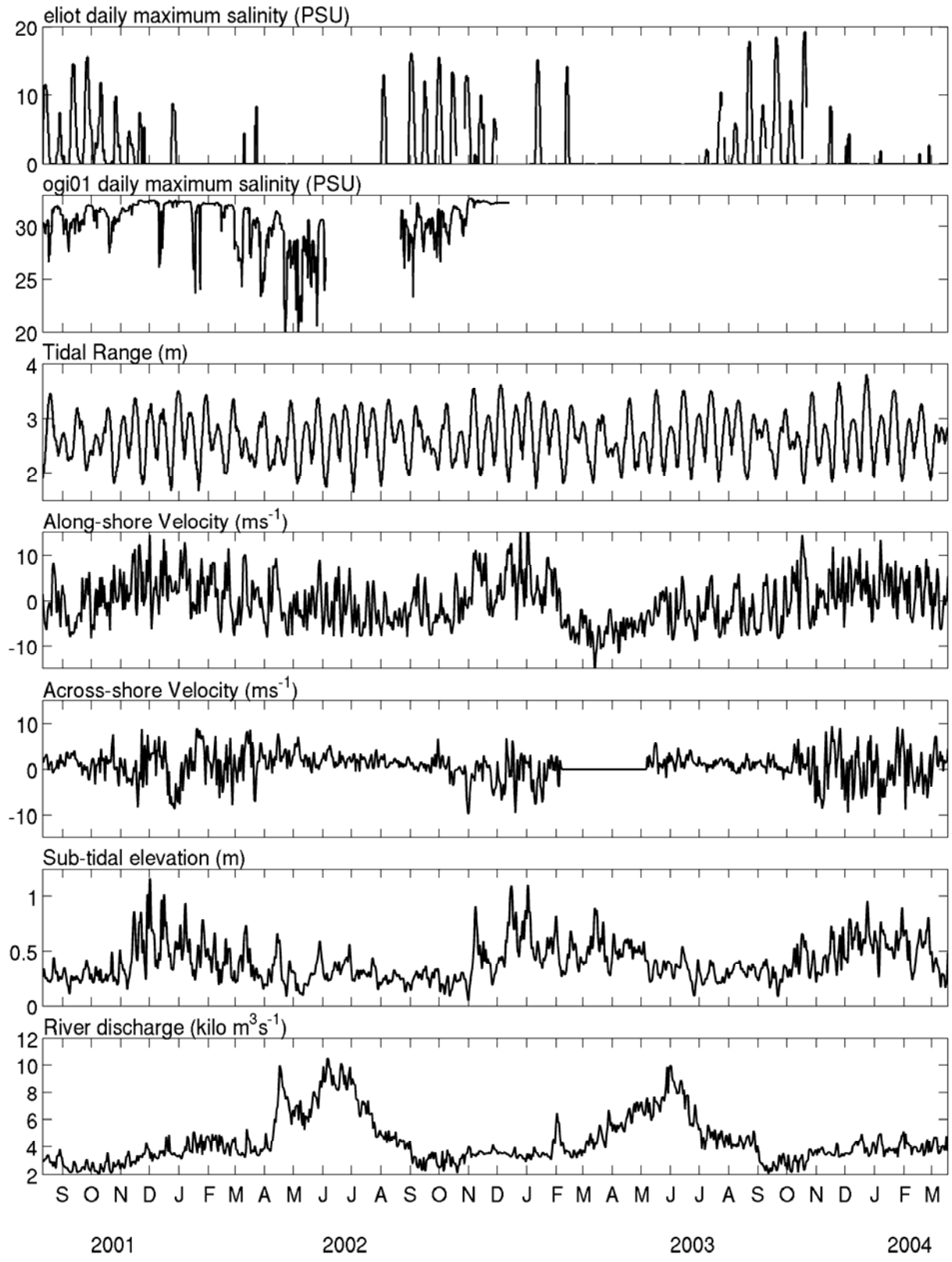
eliot daily maximum salinity (PSU)
20
10
0
ogi01 daily maximum salinity (PSU)
30
25
20
Tidal Range (m)
4
3
2
Along-shore Velocity (ms-1)
10
0
-10
Across-shore Velocity (ms-1)
10
0
-10
Sub-tidal elevation (m)
1
0.5
0
River discharge (kilo m3s-1)
12
10
8
6
4
2
S O N D J F M A M J J A S O N D J F M A M J J A S O N D J F M
2001
2002
2003
2004

Figure 10

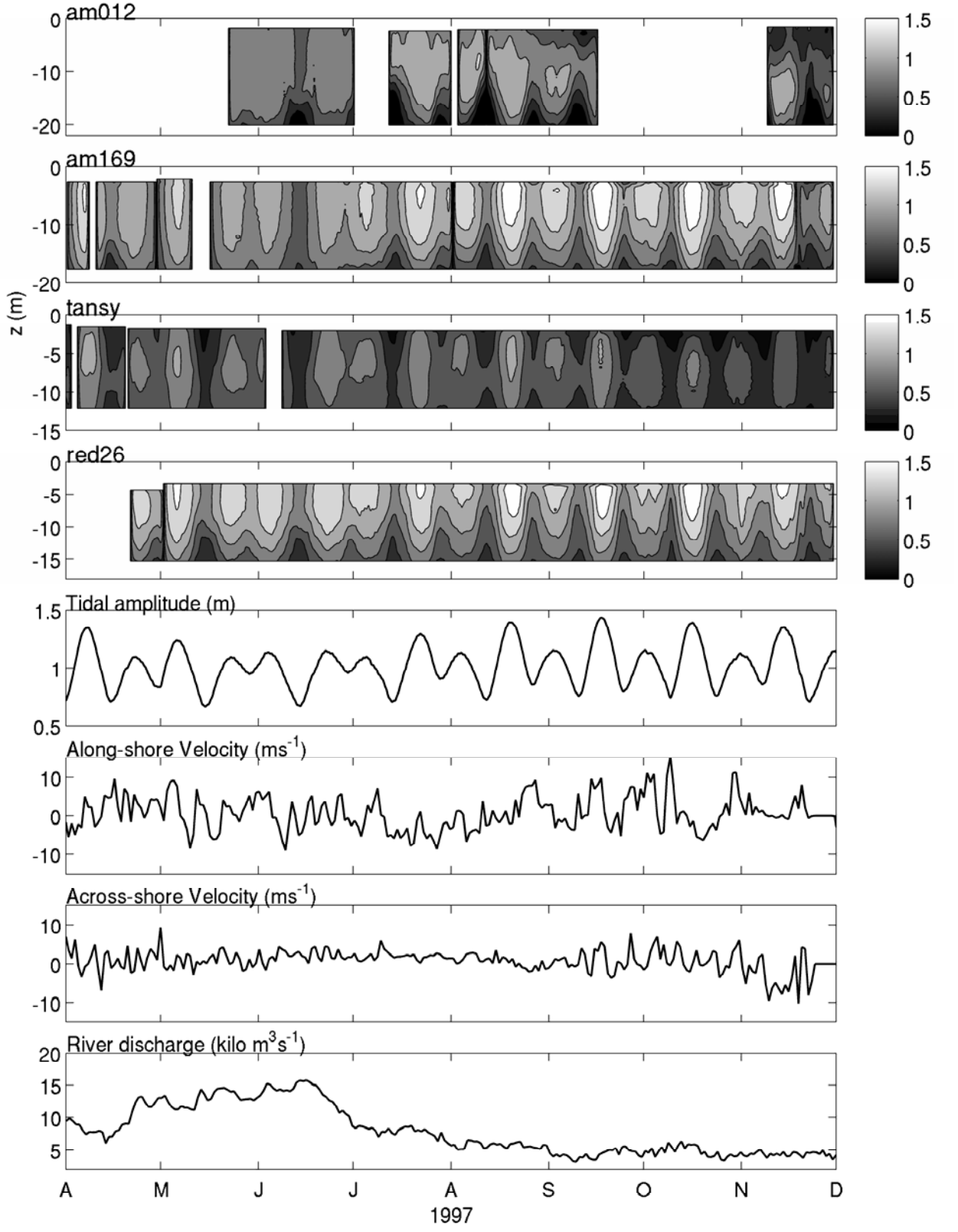
am012
am169
tansy
red26
z (m)
Tidal amplitude (m)
Along-shore Velocity (ms-1)
Across-shore Velocity (ms-1)
River discharge (kilo m3s-1)
A M J J A S O N D
1997

Figure 11

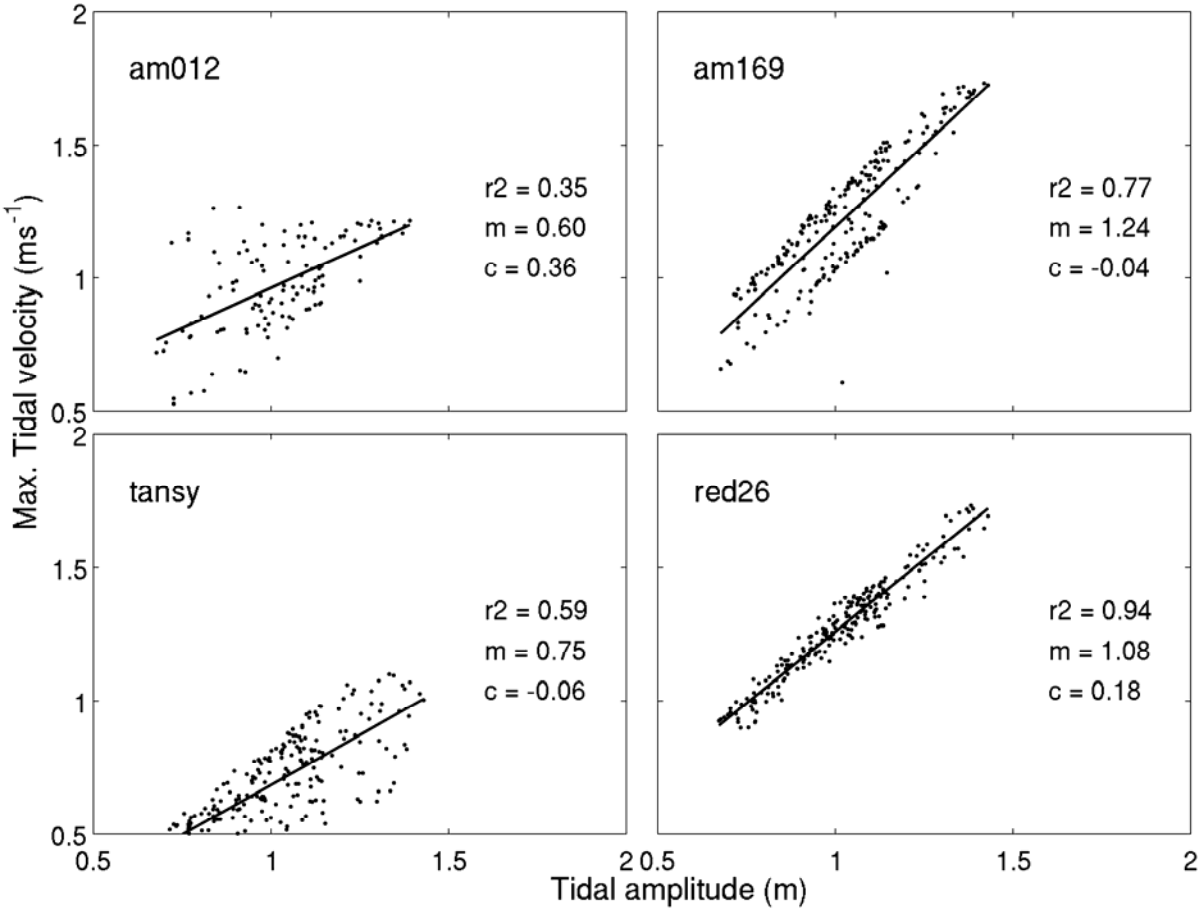
am012
r2 = 0.35
m = 0.60
c = 0.36
am169
r2 = 0.77
m = 1.24
c = -0.04
tansy
r2 = 0.59
m = 0.75
c = -0.06
red26
r2 = 0.94
m = 1.08
c = 0.18
Max. Tidal velocity (ms-1)
Tidal amplitude (m)
0.5
1
1.5
2

Figure 12

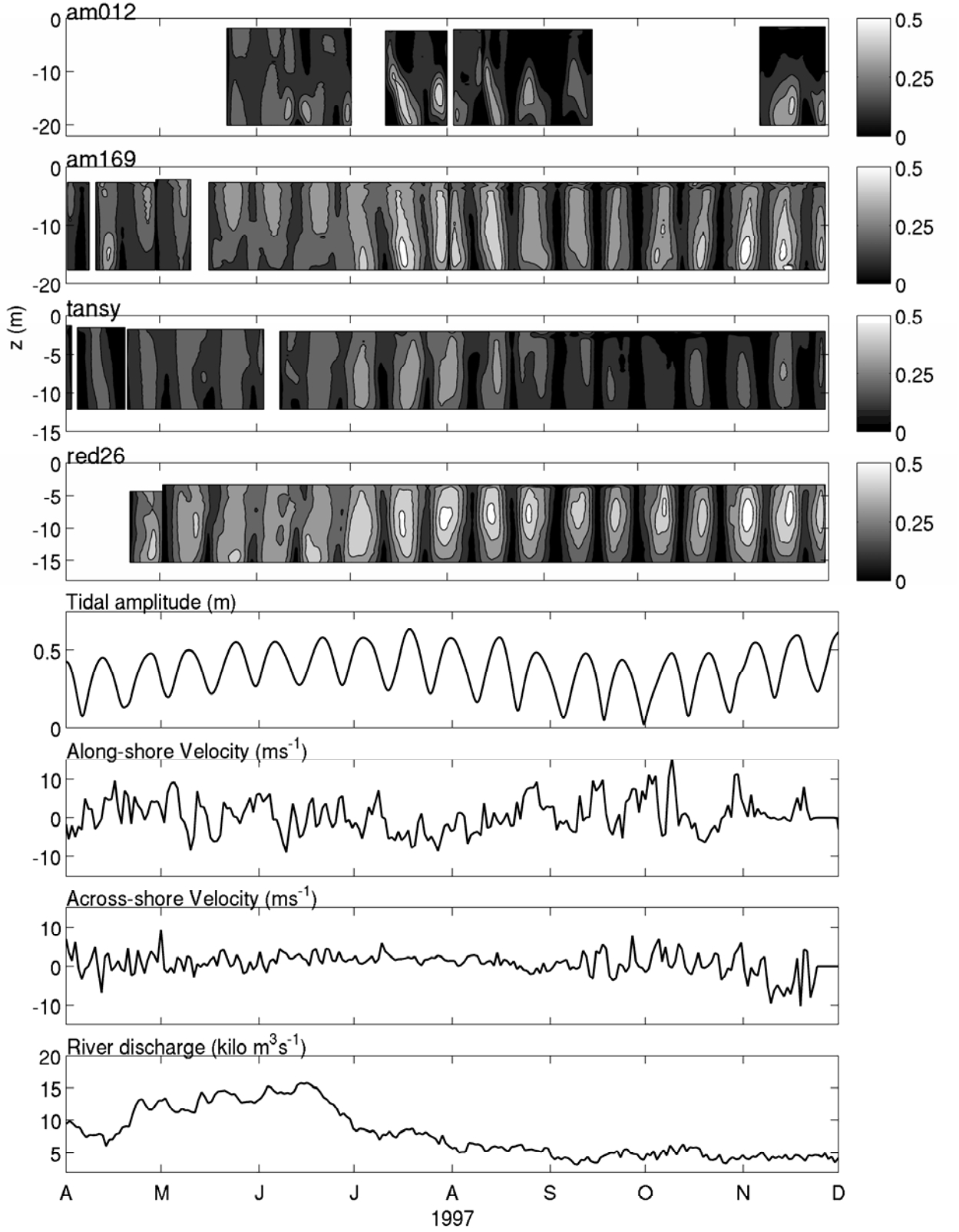
am012
am169
tansy
red26
z (m)
Tidal amplitude (m)
Along-shore Velocity (ms-1)
Across-shore Velocity (ms-1)
River discharge (kilo m3s-1)
A M J J A S O N D
1997

Figure 13

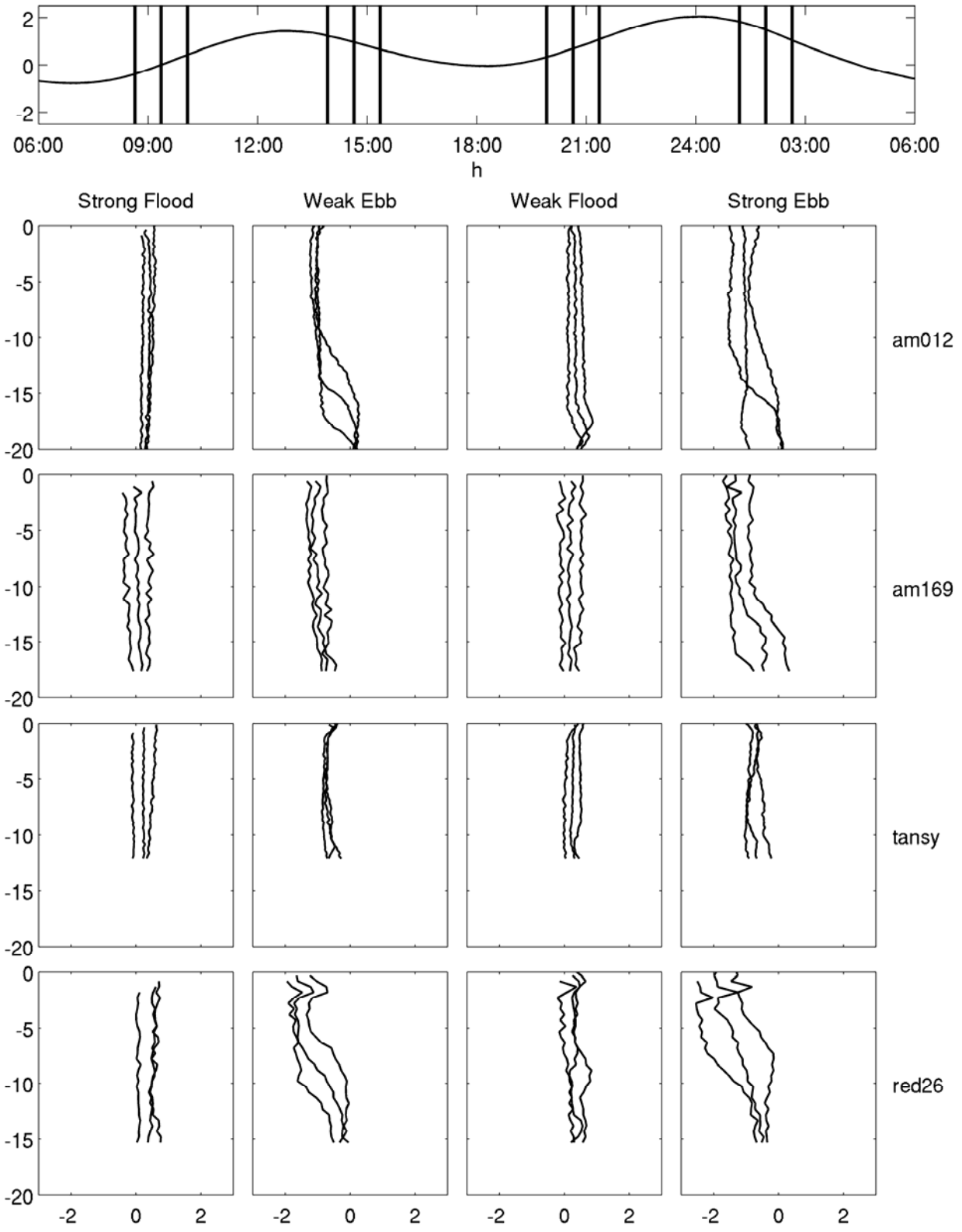
2
0
-2
06:00
09:00
12:00
15:00
18:00
21:00
24:00
03:00
06:00
h
Strong Flood
Weak Ebb
Weak Flood
Strong Ebb
0
-5
-10
-15
-20
am012
am169
tansy
red26
-2
0
2

Figure 14

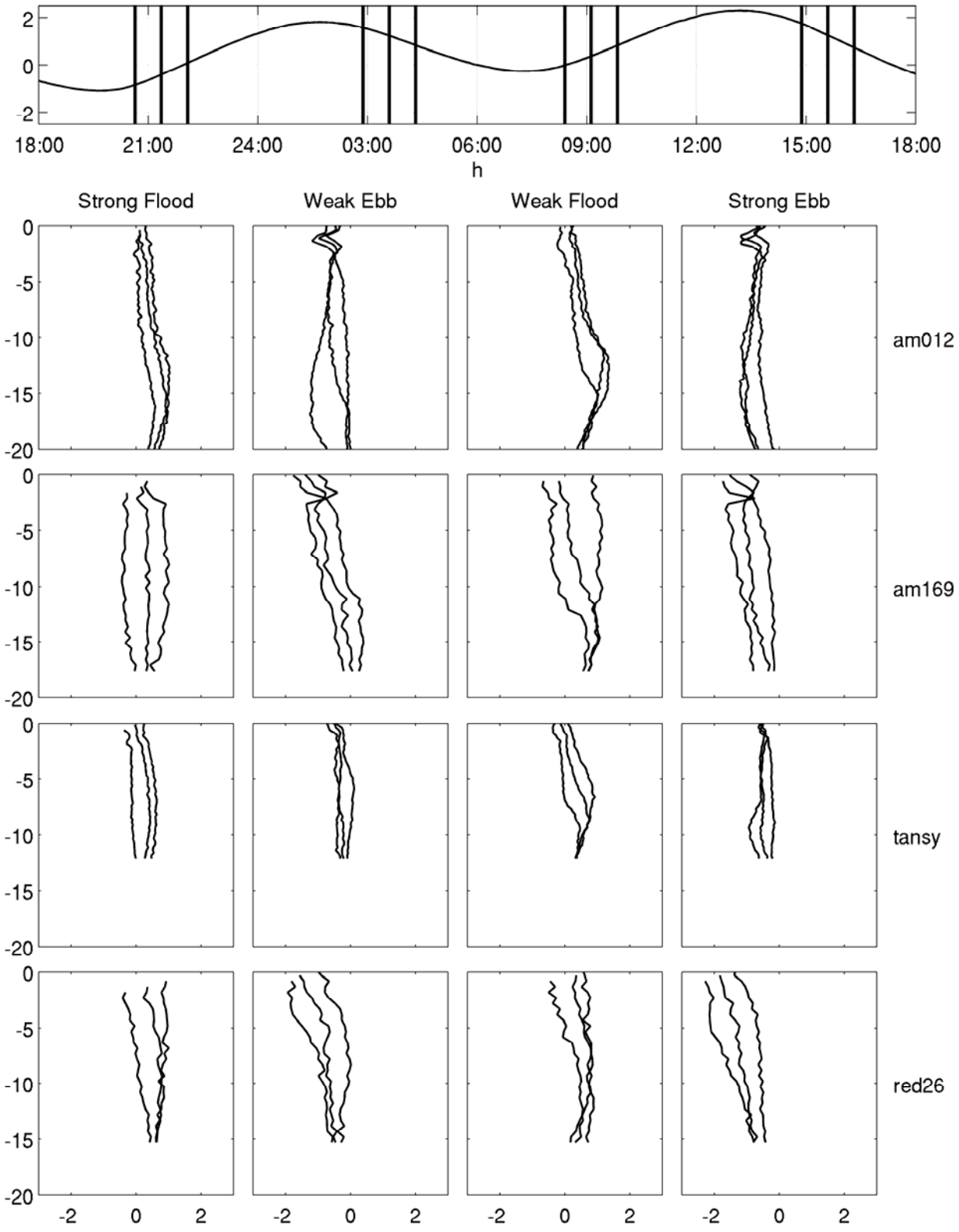
2
0
-2
18:00
21:00
24:00
03:00
06:00
09:00
12:00
15:00
18:00
h
Strong Flood
Weak Ebb
Weak Flood
Strong Ebb
0
-5
-10
-15
-20
am012
am169
tansy
red26
-2
0
2

Figure 15